Layered Double Hydroxide Protective Films Developed on Aluminum and Aluminum Alloys: Synthetic Methods and Anti-Corrosion Mechanisms

Muhammad Ahsan Iqbal [1,2], Luyi Sun [2], Allyson T. Barrett [2] and Michele Fedel [1,*]

[1] Department of Industrial Engineering, University of Trento, Via Sommarive 9, 38123 Povo TN, Italy; muhammadahsan.iqbal@unitn.it

[2] Polymer Program, Institute of Materials Science and Department of Chemical and Biomolecular Engineering, University of Connecticut, Storrs, CT 06269, USA; luyi.sun@uconn.edu (L.S.); allyson.barrett@uconn.edu (A.T.B.)

[*] Correspondence: michele.fedel@unitn.it; Tel.: +39-0461-285354

check for updates

Abstract: This work reviews the characteristics of layered double hydroxides (LDHs) in the context of protective thin films to enhance the corrosion resistance properties of aluminum alloys. A discussion is made in detail about the LDH protection mechanism and the effect of synthesis approaches on LDH structural variations and the corresponding anti-corrosion behavior. LDHs anion-exchange behavior to host inorganic/organic anions makes them a potential material to investigate for anti-corrosion film. This unique advantage and the availability of a wide range of metal oxide-based layers, interlayer anions, and self-healing properties make LDH family an attractive choice for the development of compact LDHs based smart coating systems.

Keywords: layered double hydroxide; aluminum alloys; nanocontainers; corrosion resistance; reaction mechanisms

1. Introduction

Aluminum alloys are considered optimum materials for various applications, due to their promising characteristics: for instance, conductivity, strength to weight ratio, natural abundance, and ready availability at low cost. However, aluminum alloys demonstrate compromising corrosion resistance properties and become susceptive to localized corrosion, especially pitting and intergranular corrosion, on contact with aggressive media which causes the destruction of the surface aluminum oxide protective layer [1–4]. Aluminum thin oxide layers are formed when a surface is exposed to the atmosphere. The metal remains protected unless the surface is exposed to conditions i.e., alkaline ones, which can damage the oxide layer. The microstructural features are other factors that significantly affect the properties of aluminum. Intermetallic phases are found to decrease/improve physical and mechanical properties, depending upon the distribution, type and morphologies of the phase [5,6]. Several intermetallic phase particles, like Al_3Mg_2, Mg_2Si, Al_2CuMg, and $MgZn_2$ are anodic to the aluminum matrix and corrode preferentially with respect to the aluminum matrix, while the particles like AlFeMnSi, AlCuFeMn, Al_2Cu (θ phase) and AlCuFeSi are found to be cathodic with respect to the aluminum matrix and cause peripheral trenches in the aluminum matrix adjacent to the intermetallic particles [7]. Iron, which is major class of secondary phase (AlFe and/or AlFeSi), induces a decrease of both mechanical and corrosion resistance properties but it reduces the tendency to adhere to metal molds [8]. The anodic behavior of intermetallic particles regarding the aluminum matrix can cause localized corrosion [9]. On the other hand, it is most likely that pitting corrosion or other forms of localized corrosion attack enhance fatigue

crack initiation [10]. Chromate-based conversion coatings systems have been employed for a long time to protect aluminum alloys but due to the presence of hazardous Cr(VI) groups, much attention has been paid to develop suitable alternatives [11,12]. Various coating systems, for example, anodization [13,14], sol-gel synthesis [15,16] conversion coatings [17,18], magnetron sputtering [19,20], polymer coatings [21,22] and self-assembly [23,24] are widely investigated approaches to develop non-chromate based corrosion resistance coatings. Layered double hydroxides, also referred to as hydrotalcite, are a group of anionic clays and are actively investigated in different fields due to their unique characteristics. They are generally represented by the expression $[M^{2+}_{1-x}M^{3+}_{x}\cdot x(OH)_2]A^{n-}_{x/n}\cdot mH_2O]$, where M^{2+} are divalent cations, while M^{3+} are trivalent metal cations. "A" represents the n-valent anions. The LDH structure is organized when M^{2+} is substituted by M^{3+} and A^{n-} anions are used to balance the net positive charge [25–28], and the molar ratio of $M^{3+}/(M^{2+} + M^{3+})$ range from 0.20 to 0.33 [29,30]. Due to the anion exchange capability of LDHs, various anions can be successfully incorporated inside the LDH interlayer to modify the chemistry of LDH for specific applications: for instance, supercapacitors, environmental sciences, catalysts, adsorption, etc. [31–37]. Recently, regarding the subject of anti-corrosion materials, layered double hydroxide (LDH)-based coating systems have also been widely explored, due to LDHs' peculiar morphology, a wide range of cationic/anions combinations, environmental friendliness, barrier properties, high surface to volume ratio and multifunctional design along with the capability to intercalate various species, such as metal ions of mixed valences, complex inorganic, organic molecules in the in LDH interlayers, and thus can be utilized as multifunctional coating systems. The LDHs' film thickness, number of layers, composition, surface geometry, and morphology are found to influence the ability of LDHs to encapsulate various functional groups and can be controlled with the adjustment of synthetic conditions, fabrication methodology, and initial salt concentrations etc. [38–40]. Furthermore, the interlayer anions and ratio of metal cations can largely impact orientation, crystal structure, and surface geometry [41]. A wide range of divalent metal cations (M = Mg, Ca, Zn, Ni, etc.) have been used to develop MAl-LDH on aluminum/aluminum alloys, along with various combinations of anions inside the LDHs interlayers (complex anions, corrosion inhibitors, pigments, etc.). The LDH protective mechanism includes the following key features; (a) the anion-exchange ability, (b) self-healing mechanism, and (c) barrier effect, which are found to improve the anti-corrosion properties. Considering the ion exchange equilibrium constant, the nitrate ions demonstrate the lower value in the following order: $NO_3^- < Br^- < Cl^- < F^- < OH^- < MoO_4^{2-} < SO_4^{2-} < CrO_4^{2-} < HAsO_4^{2-} < HPO_4^{2-} <$ naphthol yellow$^{2-} < CO_3^{2-}$ [42]. That's the reason a lot of research has been conducted on LDH-NO_3 where nitrate groups act as active precursors to modify the LDH chemistry with different anticorrosion inhibitors through ion-exchange and can design multifunctional coating systems for corrosion protection.

To develop a compact LDH coating system, two main strategies have been pursued: (a) loading of corrosion inhibitors/anticorrosion pigments inside the LDHs; (b) LDHs dispersed/coated with polymeric coating matrix to protect the metallic surface. This work provides an overview of the utilization of the LDHs for the surface functionalization of aluminum surfaces to develop a compact LDH based system to enhance corrosion resistance properties.

2. Synthesis of LDH on Aluminum and Aluminum Alloys

In the context of LDH-based protective coatings, coprecipitation and in situ growth methods are the widely investigated approaches with various customized reaction/host modifications to develop LDH based systems. Here, we discussed in detail these two approaches and their modifications in terms of coating resistance properties.

2.1. Coprecipitated Synthesis

The coprecipitation approach is an illustration of the ex-situ method where the LDH precursors are initially synthesized in powder form and applied on the aluminum surface by using certain techniques. The coprecipitated LDH precursors are synthesized by the combination of divalent and trivalent cationic salt solutions and exhibit advantages of high purity, crystallinity, controlled chemical

composition, and significant interaction with organic/inorganic inhibitors. On the other hand, the adhesion to the surface is inconsistent. In recent years, a number of reviews have summed up the work on the synthesis of layered double hydroxides and the parameters/conditions affecting their formation [43–48]. Theiss et al. presented a comprehensive review of the synthesis of LDHs by the coprecipitation method [48]. Recently, Bukhtiyarova et al. [41] concisely reviewed LDHs' synthesis and discussed in detail the various parameters that affect the growth of LDHs, i.e., synthetic solution pH, salt concentration, the nature of the alkaline solution (NaOH, urea, ammonia, ammonium carbonate, etc.), aging time, reaction temperature, and molar cationic ratios. The synthetic conditions—including the initial concentration of salts, crystallization time, solution pH, precipitating agents—and the ratio of divalent to trivalent cations have been found to have an influential impact on LDH structure, functional properties and crystal structure parameters [49]. To enhance the corrosion resistance properties, LDH coating systems can also be modified either with various corrosion inhibitors/anticorrosion pigments by taking the advantage of LDHs' anion-exchange properties, or by the utilization of LDHs dispersed in polymeric/organic systems. Both approaches are found to significantly inhibit the interaction of aggressive species with the substrate and actively enhance the corrosion resistance properties. The self-healing capability of LDHs also makes them a viable material to enhance the corrosion resistance properties. A detailed summary of reaction conditions and general chemistry for the synthesis of coprecipitated LDHs is listed in Table 1 for a comparative study.

Buchheit et al. initially developed a ZnAl-LDH-based coating system by using the coprecipitation method and further applied it on the aluminum 2024 alloy [50] and reported the intercalation of decavanadate corrosion inhibitor inside LDH galleries [51]. William et al. [52] synthesized ZnAl-LDH intercalated with nitrate, carbonate, and chromate and processed it on organic coated AA2024 alloy. They also investigated the various anti-corrosion pigments (oxalate, benzotriazolate, ethyl xanthate) to protect the AA2024 [53]. They also investigated the LDHs intercalated with nitrate-, carbonate-, and chromate, and dispersed in polyvinyl butyral (PVB), and applied on AA2024-T3 surface [54]. Poznyak et al. [55] developed MgAl-LDH and ZnAl-LDH loaded with different anticorrosion inhibitors (quinaldate and 2-mercaptobenzothiazolate) on AA2024 and reported the kinetics of anions released on contact with the aggressive solutions. Zheludkevich et al. [56] synthesized MgAl and ZnAl-LDH loaded with divandate anions in the LDH interlayers and investigated the controlled release behavior and corrosion resistance properties of resultants to protect the aluminum AA2024. Stimpfling et al. prepared ZnAl-LDH modified by aniline and benzene derivatives, 3- and 4-aminobenzensulfonic acid (ABSA) and 3,4-dihydroxybenzoic acid (HHBA), on organo-modified aluminum AA2024 to enhance the corrosion resistance properties [57,58]. Liu et al. [59] develop cerium-modified ZnAl-CO_3^{2-} LDH on aluminum alloy through the sol-gel approach to enhance the corrosion resistance properties.

Galvao et al. reported the effect of temperature and time on the particle growth and crystallite formation to understand the growth mechanism of LDHs developed by the co-precipitation method. They described the nature of particle growth as being consistent with an Ostwald ripening and dissolution mechanism, where extended synthesis time and temperature have found a significant effect on particle size and crystallite size of LDHs [60].

2.2. In Situ Growth Method

The in situ growth approach is considered a promising choice to develop LDHs directly on the substrate with the advantage of a more facile approach, controlled film thickness/size, distinct surface morphologies, strong adhesion between LDH and the substrate, and feasible to coat complex geometries. The successful intercalation with various inorganic/organic anions can be achieved by controlling the differential growth of LDH islands on the surface-active intermetallic/active zones. Figure 1 describes the general pattern of LDH synthesis on an aluminum substrate. The aluminum alloys act as a source of Al^{3+}, where the aluminum surface starts dissolution in a basic solution to form aluminum oxides. $Al(OH)_3$ reacts with water to form a mixture of precipitated divalent cations and OH^- on the surface of $Al(OH)_3$. The substitution of divalent cations with Al^{3+} ions results in the

coexistence of $Al(OH)_3$ and $M(OH)_2$ to form the LDH structure. On the other hand, the hydroxyl ions present inside the galleries were exchanged by the solution anions (depending on the ionic radii). LDHs formed a compact layer at LDH/interface, followed by a comparatively porous LDH network (Figure 1). Initially, Buchheit et al. developed LDH directly on the aluminum alloys as corrosion resistance films and patented that work [61].
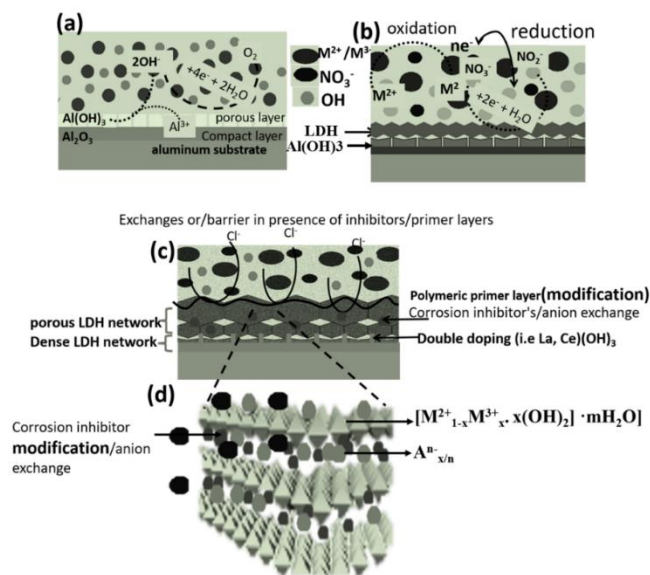

Figure 1. (**a**–**c**) Synthesis procedures of in situ growth LDH and possible modification approaches, (**d**) general representation of an LDH structure.
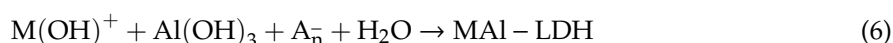
In recent years, the introduction of various corrosion inhibitors in in-situ growth LDHs has been reported (Table 1) to develop long term stable hybrid LDH/polymeric structures that were studied to achieve better stability. A polymeric primer layer can provide enough binding support and inhibit diffusion reactions. However, the basic issue of self-healing is still not thoroughly investigated in different situations, and defects/scratches may remain open for continuous interference of aggressive species with the coating systems. Recently, the concept of double-doped LDH structures was also introduced, where trivalent cations are used in LDHs structure construction (Figure 2c). High corrosion resistance is reported where cerium and lanthanum trivalent cations were used in the presence of an aluminum source [62,63]. However, the addition of larger particles inside the LDH system may cause a plasticizing effect due to the trapped corrosion inhibitors inside the LDH framework.

Synthetic conditions have many crucial parameters to control the in situ growth of LDHs; reaction temperature and aging time strongly affected the crystallinity and geometry of LDH. The pH of the synthetic solution is another factor that can influence the composition of developed LDH. For example, in the case of Zn-based LDH, it is reported that a solution pH higher than 12.6 causes an increase in the wt.% ratio of ZnO/LDH, while ZnO is found to be highly soluble in NaCl solution, thus a reduction in corrosion resistance properties is reported. Elevated pH can also cause cracks and defects and can favor the formation of secondary phases.

Surface morphology/surface area is another property that is found to have an influence on the LDH corrosion resistance properties. Various surface morphologies in that regard are reported in our previous work, for instance, platelet structure, rod-like, cauliflower-like, spiral shape, sand rose [40,64]. The SEM images of LDHs synthesis at elevated condition is reported in Figure 2 to understand the growth pattern of LDHs.

Initially at low synthetic conditions LDH granules form, which turns into net/flower-like structure at optimum conditions. Better corrosion properties were observed at extended reaction conditions (100 °C, 18 h), where a compact structure was observed compared to the traditional LDH structure [40].

The urea hydrolysis is another approach to obtain the fine distribution of crystallites and a high degree of crystallinity, but urea hydrolysis promotes the formation of carbonate ions in the system which restricts the anion exchange capabilities of LDHs [65]. Numerous aluminum substrates have been studied to develop LDHs directly on them i.e., AA2024, pure aluminum, AA6061, AA6082, AA5005, and A6N01. The anodization of substrates is found to promote higher, denser growth of LDHs with additional underlying protection. But the formation of LDH growth in such cases depends upon the PEO tortuosity and the pores which are responsible for the accessibility of the $Al(OH)_4^-$ [66]. Plasma electrolysis modification is found to develop highly stable in situ growth LDH structure and dense LDH geometry [66,67]. Meanwhile, the electrochemical deposition approach is another way to develop LDHs directly on the substrate with the advantage of controlled deposition rate and higher growth rate, but the synthetic procedure is complex and not completely discussed yet. The complete overview of synthetic approaches and relevant parameters is mentioned in Table 1 and Table 2. Synthesis of DHs can be explained with the general reactions expressed in Equations (1)–(6):

$$Al \rightarrow Al^{3+} + 3e^- \tag{1}$$

$$O_2 + 2H_2O + 4e^- \rightarrow 4OH^- \tag{2}$$

$$2H_2O + 2e^- \rightarrow H_2 \uparrow + 2OH^- \tag{3}$$

$$Al_2O_3 + 3H_2O \rightarrow 2Al(OH)_3 \tag{4}$$

$$M^{2+} + OH^- \rightarrow M(OH)^+ \tag{5}$$

$$M(OH)^+ + Al(OH)_3 + A_n^- + H_2O \rightarrow MAl - LDH \tag{6}$$

Due to elements segregation and the presence of secondary phases in aluminum alloys, a possible potential difference can form which causes the formation of corrosion microcell on the aluminum surface (Equations (1)–(3)), while hydrogen bubbles can also be formed during LDH preparation (Equation (3)). Porous outer and inner compact Al_2O_3 layers are formed and transformed into $Al(OH)_3$, which act as a precursor to form LDHs on the aluminum surface upon reaction with divalent cations. The anion exchange step further allows one to incorporate various anti-corrosion inhibitors inside the LDH interlayers and also can precipitate on the metal/LDH interface (Equations (1)–(6)) [63]. It can be said that the thickness of the LDH correlates with the number of cations, pH, reaction temperature, aging time, alkali solution and so on [41]. However, consistent values of all the describe that the morphological quality of LDH nanostructures increases with the increase of nitrate concentration in the solution. In an aqueous solution containing metallic aluminum and nitrate anions several electrochemical processes involving anodic dissolution of aluminum and cathodic reduction of nitrates and oxygen can occur. The cathodic processes generate hydroxyl ions and create a pH gradient. Although the reduction of nitrates to nitrite has been proven, there are other possible reactions involving nitrate and nitrite anions, producing nitrogen gas or ammonia, which may contribute to the overall reduction process [68] and thus can affect the film thickness as well surface morphology.

Table 1. Synthesis approaches to LDHs at various synthetic conditions with various precursors.

LDH	Anion-Exchanger	Precursors	Alkaline Media	Method	Al Alloy	Synthetic Condition °C	pH	Aging Time (h)	Ref.
ZnAl	V	ZnCl$_2$, AlCl$_3$	NaOH	coprecipitation	2024	55	6.3–6.5	12	[50]
ZnAl	V	ZnCl$_2$, AlCl$_3$	NaOH	coprecipitation	2024	55	6.3–6.5	12	[51]
MgAl	V	Mg(NO$_3$)$_2$, Al(NO)$_3$	NaNO$_3$	coprecipitation	2024	65	10	24	[55]
ZnAl	(MBT)/(QA)	Zn(NO$_3$)$_2$, Al(NO)$_3$	NaNO$_3$	coprecipitation	2024	65	10	24	[55]
ZnAlVO$_3$	-	Zn(NO$_3$)$_2$, Al(NO$_3$)$_3$, NaVO$_3$	NaOH	coprecipitated	2024	65	9.5	24	[56]
MgAlVO$_3$	-	Mg(NO$_3$)$_2$, Al(NO$_3$)$_3$, NaVO$_3$	NaOH	coprecipitated	2024	65	9.5	24	[56]
ZnAl	V	Zn(NO$_3$)$_2$, Al(NO)$_3$	NaNO$_3$	coprecipitated		65	10	24	[56]
MgAl	V	Zn(NO$_3$)$_2$, Al(NO)$_3$	NaNO$_3$	coprecipitated		65	10	24	[57]
ZnAl	4-ABSA, 3-ABSA 3,4-HHBA	ZnCl$_2$, AlCl$_3$	NaOH	coprecipitation	2024	30	9	12	[57]
ZnAlCe	-	Zn(NO$_3$)$_2$, Al(NO$_3$)$_3$, Ce(NO$_3$)$_3$	NaNO$_3$	coprecipitation	2024	65	10	18	[59]
ZnAl	Na$_2$C$_{10}$H$_{14}$N$_2$O	ZnCl$_2$, AlCl$_3$	NaOH	coprecipitation	2024	30	10	12	[58]
ZnAl	K$_2$CrO$_4$	ZnCl$_2$, AlCl$_3$	NaOH	coprecipitation	2024	30	10.5	12	[58]
MgAl	C$_6$H$_5$COON	Mg(NO$_3$)$_2$, urea	NH$_4$NO$_3$	In situ	6061	45	10	24	[72]
MgAl	8HQ	Mg(NO$_3$)$_2$	NH$_4$NO$_3$	In situ	Al	100	9	48	[71]
ZnAl*	Laurate	Zn(NO$_3$)$_2$	NH$_4$NO$_3$	In situ	Al	45	6.5	36	[70]
ZnAl	V	Zn(NO$_3$)$_2$	-	In situ	2024	<100	7	-	[69]
ZnAl*	V	Zn(NO$_3$)$_2$	NaNO$_3$	coprecipitated	2024	65	10	18	[59]
ZnAl*	V	Zn(NO$_3$)$_2$	NH$_4$NO$_3$	In situ	2024	95	6.85	0.5	[75]
ZnAl*	V	Zn(NO$_3$)$_2$	NH$_4$NO$_3$	In situ	2198	45	7	-	[73]
ZnAl*	V	Zn(NO$_3$)$_2$	NH$_4$NO$_3$	In situ	2024	95	6.5	0.5	[74]
MgAl	-	Mg(NO$_3$)$_2$, NH$_4$NO$_3$	NH$_4$NO$_3$	In situ	6082	60/80	10	24	[64]
MgAl	-	Mg(NO$_3$)$_2$	NH$_4$NO$_3$	In situ	6082	60/80/100	10	18/24	[40]
ZnAl	-	Zn(NO$_3$)$_2$, NH$_4$NO$_3$	NH$_4$NO$_3$	In situ	6082	60/80	6/6.5/7	18/24	[76]
CaAl	-	Ca(NO$_3$)$_2$	NaOH	In situ	6082	140	10	18/24/72	[77]
ZnAl	Laurate	Zn(NO$_3$)$_2$, NH$_4$NO$_3$	-	In situ	Al	85	6.5	12	[78]
NiAl	-	Ni(NO$_3$)$_2$	NaOH	In situ	6082	130	10	24	[79]
NiAl	-	Ni(NO$_3$)$_2$, NH$_4$NO$_3$	NH$_4$OH	In situ	Al	85	-	40	[80]
MgAl	-	Mg(NO$_3$)$_2$, NH$_4$NO$_3$	-	In situ	5005	125	8–10.5	1–8	[81]
MgAl	Laurate, Stearate, oleate	Mg(NO$_3$)$_2$, urea	-	In situ	Al	70	6.5	24	[82]
ZnAl	V	Zn(NO$_3$)$_2$, NH$_4$NO$_3$	NH$_4$OH	In situ	Al	120	6.5	-	[83]
MgAl	Stearic acid	Mg(NO$_3$)$_2$, NH$_4$NO$_3$	NH$_4$OH	In situ	5005	125	10	4	[84]
ZnAl-RGO	RGO	Zn(NO$_3$)$_2$, NH$_4$NO$_3$, Al(NO$_3$)$_3$, RGO	NH$_4$OH	In situ	A6N01	130–80	5.6	0.75–2	[85]
MgAl	Mo, graphene	Zn(NO$_3$)$_2$, NH$_4$NO$_3$	NH$_4$OH	In situ	2024	45	8.8	6	[86]
ZnAl	Sol gel	Mg(NO$_3$)$_2$, Al(NO$_3$)$_3$	NaOH	coprecipitation	2024	70	-	18	[87]
MgAl	Stearic acid	Zn(CH$_3$COO)$_2$	NH$_4$OH	In situ	Al	60	-	4	[88]
ZnAl	V	Zn(NO$_3$)$_2$	NH$_4$OH	In situ	2024	95	6.5	0.5	[89]
MgAl	PFDTMS	Mg(NO$_3$)$_2$	NH$_4$OH	In situ	2198	45	7	80	[90]
CoAl		Co(NO$_3$)$_2$							
NiAl		Ni(NO$_3$)$_2$							
ZnAl		Zn(NO$_3$)$_2$							
ZnAl	MBT/8HQ/V/PA/Mo	Zn(NO$_3$)$_2$	-	coprecipitation	2024	60		20	[91]
LiAl	Vanillin, aspartic acid	Li(NO$_3$)$_2$	-	In situ	A6N01	60		0.33	[92]

* LDHs layer developed over a Plasma Electrolytic Oxidation (PEO) coating.
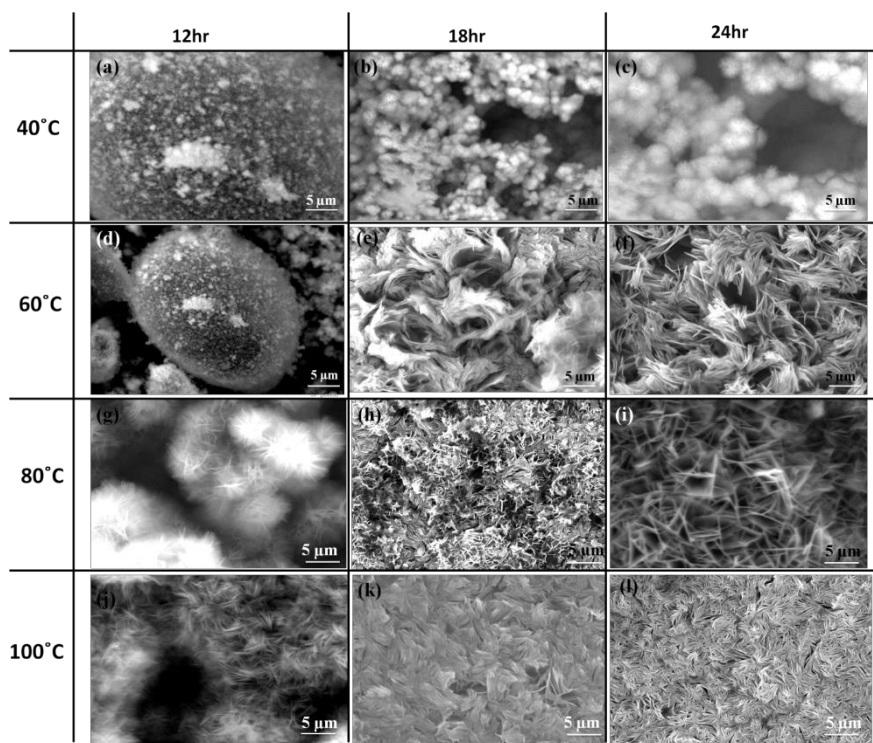
Figure 2. Effect of synthetic conditions on the growth of LDHs developed directly on the AA6082 substrate [40]: Evolution of the morphology by combining different temeratures (from 40 °C to 100 °C, vertical axis) and times (from 12 h to 24 h, horizontal axis). Image reproduced with permission from the publisher (MDPI).

3. Corrosion Resistance of LDH Films

Among the possible solutions, LDHs incorporated with corrosion inhibitors seem to be a feasible choice to protect the metallic surface, while the compatibility with organic matrices makes them a powerful option to provide long term stability and to effectively reduce the corrosion rate.

3.1. Corrosion Resistance of In-Situ Grown LDHs

LDH-based coatings have been pursued to achieve high corrosion resistance. The mechanisms through which these materials can provide the underlying substrate with improved corrosion resistance are manifold. In addition to being a physical barrier against water and ions migration, LDH-based coatings are recognized for their capability to encapsulate functional species in between the charged lamellae. As a result of this specific property, coatings based on these materials have a self-healing potential if proper corrosion inhibitors are embedded and released in situ upon a specific trigger. LDH coatings commonly show a two-layered structure (schematically depicted in Figure 3): an inner relatively compact layer and an outer porous layer formed by the interconnection of the different platelets.

Figure 3 depicts a schematic representation of the LDH coatings as well as a FIB-SEM image of the section of MgAl-LDH coating developed on AA6082. Liang et al. described the formation of LDHs on AA2099-T83 Al–Cu–Li alloy, and further explained the role of intermetallic particles on the formation of LDHs and on their corrosion resistance properties. Iron-containing intermetallic particles act as a preferential site for the formation of nucleation and growth of LDHs and a compact, uniform LDHs layer is developed on the aluminum surface [93]. Overall, intermetallic particles which are cathodic compared to the matrix, contribute to the formation of LDHs. Due to the localization of the cathodic reactions in correspondence with the intermetallic particles, LDHs nest-like morphology [64] is observed.
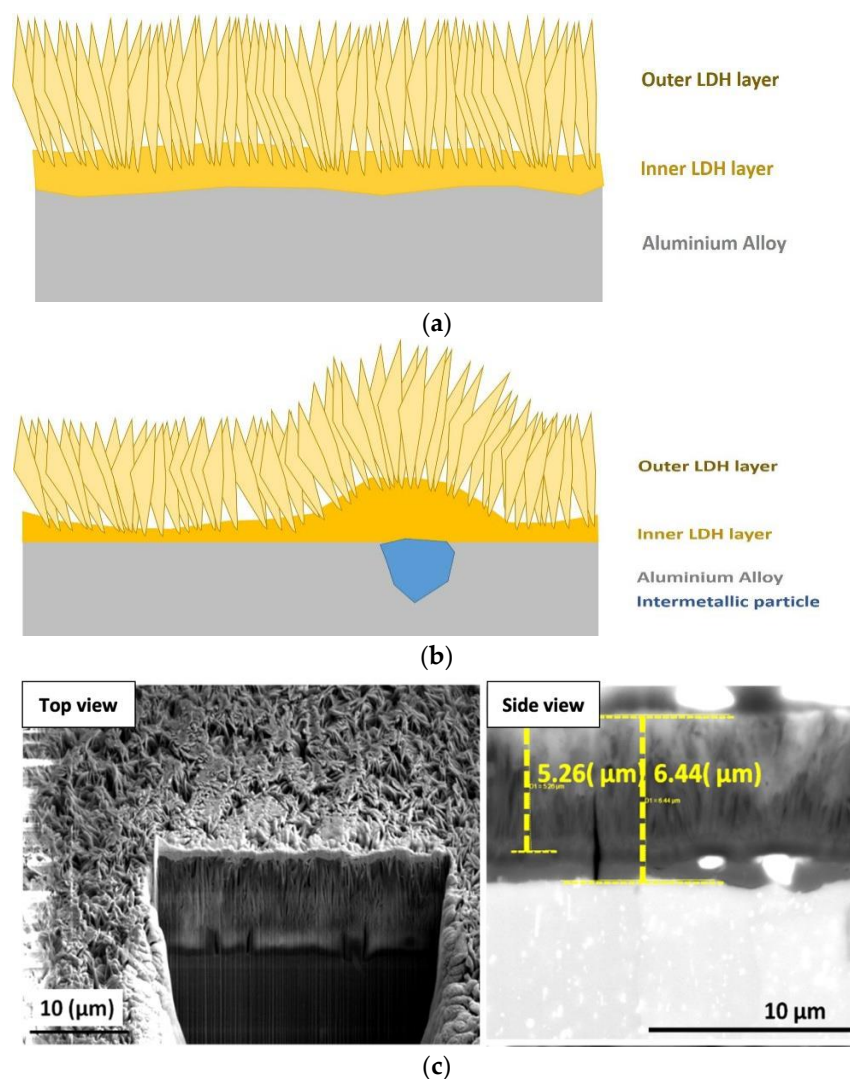
Figure 3. Structure of LDH based coatings: (**a**) schematic representation of the structure of the film; (**b**) schematic representation of the structure of the film in presence of intermetallic particles; (**c**) FIB-SEM image of MgAl-LDH coating on AA6082 (courtesy of Jönköping University).

Notice that in correspondence of the active intermetallic particles (Figure 3b), a differentiated growth of island-like LDHs occurs [60]. The inner compact layer is responsible for the physical barrier effect of the coating while the platelets, which form the outer layer, mainly provide the ion exchange reactions.

Regardless of the synthesis technique employed for the development of LDH films either by the in-situ method or the two-step method, LDHs suffer from corrosion induced by halogen ions such as chlorides. The film thickness and compactness cause an increase in LDHs barrier properties and help to reduce the diffusion of aggressive media to interact with the substrate. The film thickness can be controlled with synthetic conditions and can be modulated from a few microns to several micrometers. In our recent study, we observed that corrosion resistance varies with the effect of film thickness and high film thickness may cause a reduction of corrosion resistance due to higher porosity [40,76,77,88]. The durability of LDH coatings can also be increased with embedding corrosion inhibitors in between the platelets. In this regard, coatings based on Zn, Ca and Mg were developed directly or indirectly on aluminum substrates and have been tailored by entrapping various functional species. LDHs anion exchange reactions are generally assumed to take place too tactically, even if precipitation mechanisms have been also proposed [94,95]. Nitrate-based LDHs might be a possible

option to enhance the corrosion resistance by trapping the chloride ions through anion exchange process and release corrosion inhibitors [96]. Tedim et al. [96,97], described the synthesis of ZnAl-LDH (NO_3) and ZnAl-V-LDH developed on AA2024 and the chlorides entrapment capability of LDH-NO_3 and possible diffusion process which affects the stability of the coating against corrosion and leads to the damaging of the LDH/substrate interface.

LDHs with intercalating corrosion inhibitors are a better choice, as they are expected to deliver the inhibitors upon damaging of the matrix and can provide self-healing properties. Vanadate-exchanged LDHs were utilized by various research groups, either directly on the aluminum substrate (in-situ) or co-precipitated on the substrate, but, in both cases, the vanadate's were found to enhance the corrosion resistance of LDH [17,45,50,51,69,73]. In another work, on AA2024 substrate, ZnAl-LDH was synthesized and modified with 2-mercaptobenzothiazole and further treated with hydrophobic hexadecyltrimetoxisilane in order to functionalize the surface to obtain significant anti-corrosion and anti-biofilm characteristics [98]. To enhance the corrosion resistance properties of LDH, Zhang et al. [86] designed a graphene-based LDH, where graphene is found to act as sealing the LDH pores and improve barrier properties while MoO_4^{2-} corrosion inhibitors further help to provide a stable corrosion resistance system. Kaidong et al. [92] introduced LiAl-LDH modified with disodium vanillin L-aspartic acid to protect the A6N01 aluminum alloy. The developed coating demonstrated an enhanced corrosion resistance compared to the bare Al alloy, but pitting corrosion after 120 h of exposure in 3.5% NaCl solution was observed to take place in the presence of coating defects. CaAl-LDH was introduced by our group [77] and found to improve corrosion resistance with limited long term stability. Wang et al. [82] investigated superhydrophobic LDH coatings produced by modifying the chemistry of LDH by intercalating with oleate, stearate and laurate groups in order to modify the LDH hydrophilic nature to superhydrophobic. A remarkable improvement of the microbiological corrosion resistance properties was achieved, and such systems have shown the potential to retard the biofilm formation and significantly enhance the corrosion resistance properties. Chen et al. [99] demonstrated a simple approach to prepare an oriented NiAl-LDH on PAO/Al substrate and further modify it with sodium laurate solution to endorse super-hydrophobicity. Wang et al. [100] synthesized superhydrophobic MgAl-LDH directly on AA6061 alloy and achieved specific characteristics by modifying the LDH chemistry with triethoxy-1H,1H,2H,2H-tridecafluoro-n-octylsilane to obtain superhydrophobic LDH properties. They showed that improved mechanical and electrochemical stability can be achieved by this method, along with high durability and anti-icing properties. LDHs also exhibited the so-called shape memory effect, where calcination causes dehydroxylation and decomposition of anions inside the galleries. Calcination strongly affects the oriented growth of the LDH, causes an increase in the surface area and contraction of the basal spacing, and increases the likeliness for anion exchange, which in turn causes a compact structure that substantially influences the LDH corrosion resistance properties [101]. To promote the barrier properties, the synthesis of LDHs on the anodized aluminum substrate can provide significant active and passive corrosion protection to obtain a compact coating system [90]. Conceptually, the LDHs grown on the anodic film may seal the micropores of the anodized surface (strong barrier properties), and LDHs itself provides active protection via entrapment of aggressive species and through self-healing properties [75]. Moreover, LDH preferentially grows on the entire surface of the anodic film including the bumpy areas and on the complicated surface providing a suitable approach to protect the aluminium alloys [102]. Recently combined effect of LDH coatings grown on a "plasma electrolytic film" have become an interesting research area due to combined attractive properties of active and passive protection [74,89,103].

Rare earth elements are found to have a significant inhibiting effect and are the object of considerable scientific interest [104], and generally exhibit a non-toxic nature [105]. Among rare earth elements, cerium-based coatings attract significant attention, specifically in case of incorporation inside the LDH network [59]. The synthesis of LDHs on anodized aluminum alloys is also reported and successfully proven helpful to develop a comparatively stable protective system where anodization of Al alloy support to develop a dense network of LDHs, and also the LDH solution treatment causes the sealing

effect of anodized surface, and such synergistic effect is found to improve the corrosion resistance of Al alloys [73–75]. Li et al. [73] developed ZnAl-LDH modified with vanadate corrosion inhibitors directly on anodized 2198 alloy and reported the long-term stability of the LDHs system. Kuznetsov et al. [75] developed an LDH-based sealing method for anodized AA2024. AA2024 sheets were grounded and anodized in a solution of 0.53 M $C_4H_6O_6$, 0.46 M H_2SO_4 at 37 °C for 25 min with an applied voltage of 14 V. It demonstrated the corrosion protection performance of actively sealed anodized aluminum surface with smart nano-containers. From the above discussion, we can say that composite hybrid LDH systems can provide multifunctional coating systems and can provide self-healing, self-wash ability, and biocompatibility as per applications. However, to analyze the LDHs self-healing capability and further, the response time and release rate of embedded inhibitors is still an issue and very little work is reported on that topic. This is discussed in more detail in Section 3.3.

3.2. Corrosion Resistance Co-Precipitated LDHs in Organic and Hybrid Matrices

LDH dispersions in polymeric matrices (see schematic representation in Figure 4) have been studied in order to enhance the coating stability against corrosion and provide better mechanical properties along with stress dissipation ability. In order to achieve an enhancement in terms of corrosion properties, LDH particles are embedded inside an organic or organic/inorganic hybrid (OIH) matrix in order to: (1) act as a physical barrier against moisture and oxygen permeation and (2) provide a controlled release of corrosion inhibitors. layered double hydroxides dispersed inside a polymeric matrix improves the barrier properties of organic coatings by increasing the length of the pathway water and other species take to reach the metal interface, similar to other lamellar pigments [106].

ZnAl-LDH intercalated with EDTA via co-precipitation and further coated on AA2024 was discussed and the capability of EDTA for anion exchange and corrosion resistance behavior is reported and the nature of ZnAl-CrO_4-LDH, ZnAl-CO_3-LDH, ZnAl-Cl-LDH are completely revealed [58]. Liu et al. [59] developed the cerium based LDH protective system with the combination of hybrid sol-gel on aluminum 2024 alloy and described the synergistic inhibiting effect of ZnAlCe-LDH and CeO_2 nanoparticles on the corrosion resistance properties of aluminum.
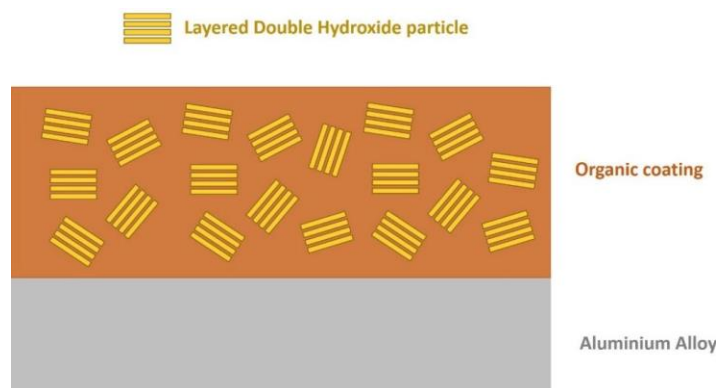

Figure 4. Schematic representation of the co-precipitated LDH dispersed into an organic coating.

The inhabitation effect of MgAl-LDH mixed at various proportions with hybrid sol-gel compose of (tetra-n-isopoxyzirconium (TPOZ) and 3-glycydoxypropyltrimethoxysilane (GPTMS)) were synthesized, and enhancement in corrosion resistance was monitored [87]. In another work, molybdate-intercalated MgAl-LDHs were synthesized by the coprecipitation method, dispersed in water-soluble (polyvinyl alcohol) PVA polymeric matrix, and the composite matrix coated onto Al5054 alloy. The prediction model was also introduced to estimate the release profile of the inhibitor from LDH [107]. Luo and coworkers [85] developed thin ZnAl-LDHs by the hydrothermal method on 6N01 Al alloy, and to inhibit the chloride penetration, oxygen diffusion, and prevention of water interaction, reduced graphene oxides sheets were used to seal the porous LDHs layers. The system

provides very good corrosion protection owing to the barrier function, ion exchange, and self-healing ability. The reported examination remarks upon recent approaches in introducing sharp anti-corrosion functionalities in protective coatings, utilizing guest reservoir carriers of corrosion inhibitors. A thick PLA coating was used to seal the porous outer layer of the LDH coating provided a strong adhesion. A delay was found in the penetration of aggressive ions inside the composite coating which in turn provided longer protection. Subasri et al. [91] reported a comparative study of the utilization of various corrosion inhibitors in different proportions for instance, vanadate group, 2-mercapto benzothiazole, 8-hydroxyquinoline, phytic acid intercalated LDH and studied the effect of resultant dispersion in the sol-gel matrix to investigate the compactness and corrosion resistance properties of LDH to protect the AA2024 substrate. After 120 h salt spray exposure to 3.5% NaCl solution, ZnAl-LDH with corrosion inhibitors of phytic acid and 8-hydroxyquinoline were seen to show the lowest corrosion current densities. Another possible choice is the dispersion of LDHs in polymeric matrices which results in better mechanical and electrochemical properties and facilitates the barrier properties. Zhang et al. [108] synthesized Ce-doped ZnAl-LDH further dispersed in sol-gel matrix and applied on AA 2024 to enhance its corrosion resistance properties. The findings depicted that Ce ions were actively incorporated in LDH galleries and sol-gel modified ZnAl-Ce-LDH delay the degradation process on exposure with aggressive species and can be used as potential a corrosion inhibiting system with self-healing properties. The following progression is generally observed regarding the corrosion resistance properties of virgin LDHs; Mg–Al-LDH > Zn–Al-LDH > Li–Al-LDH > Ca–Al-LDH.

3.3. Kinetics and Controlled Release of Interlayer LDHs Corrosion Inhibitors

Corrosion inhibitors entrapped inside LDHs' interlayers play a vital role to inhibit corrosion reactions, which is why the kinetics and understanding of inhibitors release rate on contact with aggressive species are crucial factors to develop a stable coating system. The controlled release rate of LDH anticorrosion inhibitors under different reaction stimuli and the self-healing capability predict the lifetime of LDH systems. Slow or/fast anion exchange speed caused either short time stability or poor corrosion resistance. It is found that the healing process depends on various factors, mainly on the film thickness, elastic modulus, dimension of the damaged area and so on and can be explained by mathematical models and theoretical expressions. Further, Mohar's approach can be used to predict the chloride contents after LDH exposure with an aggressive solution to understand the anion exchange and system predictability [79]. Weight loss measurements (ISO 8407 Standard) [109] before and after intercalation of corrosion inhibitors and concentration gradient measurement also proposed predictability to measure the corrosion rate and kinetic modeling combined with physical characterizations.

Recently Imran et al. reported a prediction model and kinetics study to analyze the inhibitor release profile, where Fickian diffusion is considered as a molybdate release rate and the data were fitted with the Weibull model to study the MgAl–Mo-LDH/PVA behavior on contact with 3.5% NaCl [107]. Bendinelli et al. [110] investigated the release rate of MgAl-imidazole-LDH and analyzed the inhibiting efficiency and studied the interparticle diffusion model to understand the kinetics and release rate of inhibitors. The synthetic parameters, structural geometry, and pH of the contact solution are the prime parameters to affect the inhibitor's release rate with physical characterization approaches, like basal spacing differences through XRD. Very few reports are published on that issue and there is a need for further investigation on those criteria for the reason of practical implementations of LDHs coatings. Although the studies cited do not refer specifically to the LDHs corrosion inhibitors kinetics, the following literature provides an idea of the kinetics measurement and modeling to predict the release rate and kinetics of different anions inside the LDHs galleries [111–113].

3.4. Testing and Evaluation of LDH Coatings or Co-Precipitated Particles

Electrochemical Impedance Spectroscopy (EIS) is considered a basic approach to evaluate the coating properties and barrier properties. In fact, impedance measurements are recognized to supply

valuable information about protective coatings applied on metals and about their degradation mechanism, as well [114–116]. Impedance modulus and impedance phase graphs (quite often referred to as "Bode plots") and Nyquist plots are used to show the impedance spectra collected over coated metals immersed in different electrolytes. From these graphs it is possible to gain a preliminary knowledge of the protective properties of the coatings: scientists refer to the modulus of the impedance in the low-frequency range (commonly in the 0.015–0.010 range) as a rough estimation of the quality of the protection system, in accordance with the claims of Bacon [117] and Murray and Hack [118], as highlighted by Amirudin and Thierry in their review [119]. In order to get some insight into the mechanisms through which coatings are able to protect the substrate, very often the experimental EIS data are studied by means of the nonlinear least-squares fit technique [116,120] which has been recognized to be a valuable tool for analyzing complex frequency dispersion data [121]. For this purpose, passive circuit elements (called "e.e.c., electrical equivalent circuits") are commonly employed to fit impedance data arising from different experimental systems. Despite the implicit ambiguity claimed by McDonald [122] for the different possible geometrical arrangements of the circuit elements, the exploitation of the e.e.c., for the fit of an experimental set of EIS spectra is definitely widespread. In this context, LDH developed in situ on aluminum alloys have been often investigated by EIS and diverse e.e.c., have been suggested by different groups to fit the EIS experimental data and to assess the corrosion protection properties of the coatings. Various equivalent circuits were used due to the dynamic nature of LDH coating systems, where capacitance is replaced generally by constant phase element (CPE), which describes the non-homogenous nature of the LDH system and how it deviates from the ideal capacitive behavior. CPE approach is used extensively in equivalent circuits for fitting the experimental data and is attributed to the surface activity, inhomogeneity, factual geometry, roughness, electrode porosity, etc. It is believed to describe the current and potential distribution associated with the electrode geometry [123].

Wang et al. [64] introduced the circuit depicted in Figure 5a to fit the experimental EIS data of MgAl-LDH developed on 99.9% Al. In the model employed by the authors, *Rs* refers to the solution resistance, $R_{pore,}$ and CPE_{pore} to the conductive path in the films and double layer capacitance in the pores of the films, respectively; R_{ct} and CPE_{dl} to the polarization resistance and double-layer capacitance, respectively; R_{film} to the inner film resistance and CPE_{film} the constant phase element of the film.

A similar circuit (depicted in Figure 5b) has been proposed by Zhou [63] for the interpretation and fit of the EIS data set collected over ZnLaAl-LDHs developed on AA6061. Also, in this case, the presence of a three-time constant has been suggested. A time constant has been attributed to the Faradic process and modeled by a charge transfer resistance, R_{ct}, in parallel with the double layer capacitance (CPE_{dl}); a second time constant has been related to the oxide film between the aluminum substrate and LDHs: R_{OX} represents the resistance of film in parallel with the capacitance (CPE_{OX}); a third time constant has been introduced to account for the contribution of the LDH layer itself: the LDHs film resistance (R_{LDH}) in parallel with the layer capacitance (CPE_{LDH}). Similarly, Tedim et al. [69] identified three-time relaxation processes in the EIS spectra collected over ZnAl-LDHs on AA2024. The time constant in the high-frequency range has been associated with the LDH layer response, a second-time constant attributed to the aluminum oxide present on the alloy surface, and a third-time constant attributed to the corrosion process. The same authors suggested a similar circuit (depicted in Figure 5b) [97].

Wang [100] introduced two relaxation processes e.e.c., (Figure 5c) where R_s represents the solution resistance; R_{ct} and R_f are the charge transfer resistance and the film of the MgAl-LDHs resistance, CPE_f and CPE_{dl}, are the capacitance of the LDH film and the electrical double layer, respectively.

A two-time constant model (Figure 5c) has been employed also by Liang et al. when investigating the properties ZnAl-LDHs on AA2099 [93]. According to the attribution given by the authors, in addition to the resistance of the electrolyte R_S, R_f and CPE_f represent resistance and component of the constant

phase elements of the LDH/natural alumina film, respectively; R_{ct} and CPE_{dl} (charge-transfer resistance and component of the double layer constant phase, respectively) account for the faradic process.

Our impression is that among the different models to fit the EIS raw data set, the main difference resides in the interpretation of the contribution of the LDHs layer itself. In Section 3.1 it has been explained that the LDHs films consist of a barrier inner layer and a porous outer layer. In the literature, sometimes it has been possible to discriminate the contributions of the two different layers and, therefore, the e.e.c., like the ones depicted in Figure 5a,b are employed. In this case two different relaxation processes that can be attributed to the two different layers of the LDHs coatings are present in the EIS spectrum. Additionally, as far as the literature reports examined in this work are concerned, a time constant attributed to the corrosion process is always present (described by R_{ct} and CPE_{dl}). In other cases, the overall contribution of the LDHs film has been interpreted as a single relaxation process and therefore modelled employing the circuit depicted in Figure 5c. Also in this case, an additional time constant to account for the corrosion is present (described by R_{ct} and CPE_{dl}). Basically, both interpretations can be correct: it depends on the physical properties and morphological features of developed LDHs films. In fact, it is not always possible to clearly discriminate the different contributions of the two layers forming the LDHs film. For example, if the outer layer is very porous or very thin, its contribution to the EIS spectrum can be strongly reduced or negligible. Generally speaking, it is our opinion that a deep understanding of the physical and morphological structure of the developed LDHs film is needed to properly select the suitable e.e.c., which aims to fit the EIS raw data set.

As far as LDH dispersions in polymeric matrices are concerned, EIS spectra are fitted employing the well-established e.e.c., developed for organic coatings [118,124,125]. In particular, ionically conducting low resistive paths in the coatings, due to discontinuities or defects, are modeled with a resistance (namely "porosity resistance", "pore resistance", R_{po}) [126]. The dielectric behavior of the coating is modeled employing a pure capacitance (namely "coating capacitance", C_c). The corrosion process occurring under the paint is modeled employing a charge transfer resistance (R_{ct}) in parallel with a double layer capacitance (C_{dl}). It has to be underlined that in some cases the response of an aluminum/coating/electrolyte system is also modeled employing a CPE which accounts for an oxide layer existing on the aluminum alloy electrode instead of the time constant attributed to the faradic process (R_{ct}, C_{dl}) [127].

In Table 2, the resistance of in situ developed LDHs obtained from the fitting of the experimental data set collected by different authors is listed. In particular, the value of R_{pol} and R_{coat} are reported. The evolutions of pore resistance in the case of LDH provide a framework about the barrier properties and describe the dispersibility and compactness of LDH in the composite system. Regardless of the specific e.e.c., employed to model the physical properties of the LDH coating under investigation, a possible way to compare them in situ developed LDH layer is to employ the total resistance R_{tot}. This parameter corresponds to the sum of the resistance values obtained through the fitting and can be assumed as a sort of overall estimation of the protection extent of the LDH layer. A detailed comparison of literature data is not possible since the thickness of the different LDH protection layers is very different from one author to another and quite often the value is not reported at all. However, we calculated the R_{tot} values of the in-situ developed LDH coatings on different aluminum alloys (mainly pure aluminum, AA6xxx, and AA2xxx) of different authors and we compared the obtained results with the R_{tot} of the same system intercalated with corrosion inhibitors. Figure 6 shows the obtained results in the case of samples exposed in chloride-containing media (from 0.1 M to 3.5 wt.% NaCl) for a few hours. The huge dispersion of R_{tot} data both for pristine and inhibitors containing LDH is due to the wide range of thicknesses of the different coatings. In addition, diverse concentrations in NaCl in the electrolyte have been used by the different authors (notice that as far as the literature reports considered in this review are concerned, no clear trend of R_{tot} with the chloride content has been found). However, notice that the LDH layer without any inhibitor ranges from 10^2 to 10^8 Ω cm^2, while in presence of a corrosion inhibitor the R_{tot} values tend to increase (they range between 10^3 to 10^{12} Ω cm^2). These results, taken from literature reports, suggest that, in general terms, it is possible to

significantly increase the corrosion protection properties of LDH layers by exchanging the anions in the lamellar structure with corrosion-inhibiting species.
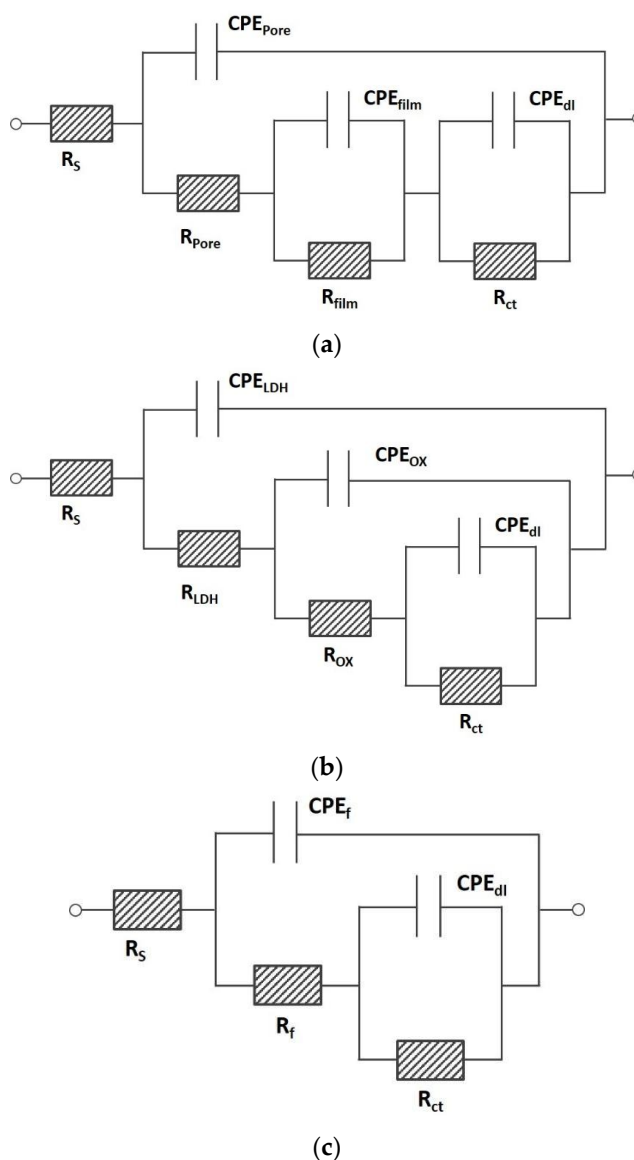

Figure 5. Schematic of the circuits employed to fit the experimental data set of LDH coatings developed on aluminum alloys: (**a**,**b**) three-time constants and (**c**) two-time constants.

Polarization curves are also quite often collected over LDH films developed on aluminum alloys to assess the corrosion protection properties. According to the mixed potential theory, anodic and cathodic reactions can be described by a straight line in the E versus Log(i) plot. For purely activation controlled anodic and cathodic processes, a linear extrapolation of the Tafel slopes from the experimental curves is possible [128], thus determining the corrosion current density. When one of the reactions (generally the cathodic reaction) is limited by the rate of transport of the reactant to the metallic surface (concentration-controlled processes) the extrapolation of the corrosion current density is still possible, even if it becomes more complex. If a dielectric coating is present over the metal surface, the ohmic drop due to its insulting nature affects the reliability of the Tafel extrapolation of the corrosion current density. In addition, the extrapolation of corrosion current density values over passive metals such as aluminum in a near-neutral chloride containing media is of doubtful scientific significance. However, there are many literature reports in which the corrosion current density is extrapolated

from E versus Log(i) plots in presence of a dielectric film (LDH coating or organic coating) over the surface of aluminum electrodes immersed in neutral chloride containing media (see the References in Tables 2 and 3). It is our opinion that DC polarization curves collected over coated aluminum samples can provide mainly a qualitative assessment of the quality of the coatings. The flow of direct current in the case of metals coated with insulating materials is mainly possible thanks to the presence of defects and/or heterogeneity through which the electrolyte can reach the metallic surface. Therefore, the evolution of the anodic and cathodic current densities can be related to the amount of defect and homogeneity of the coatings.
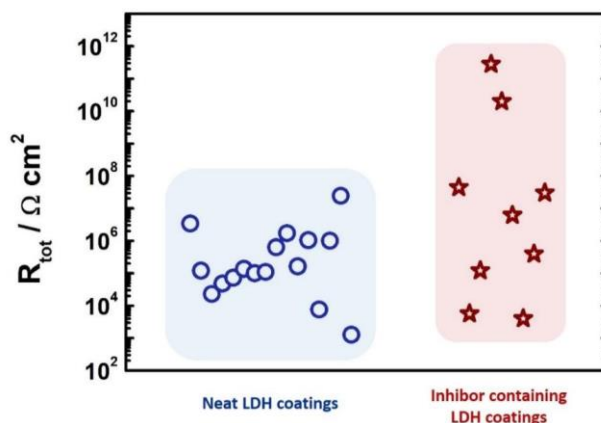

Figure 6. Comparison of the total resistance obtained from EIS spectra fitting for neat and inhibitor exchanged LDH coatings; data taken from [102–117].

Despite our concerns, it must be highlighted that current density data are extrapolated by many different authors from the potential/current density plots collected over LDH or paint coated aluminum alloys, as reported in Tables 2 and 3.

DC techniques and EIS provide a general description of the LDH system but these techniques refer to the average surface response, and localized defects cannot be truly estimated by those approaches. Spatially resolved electrochemical techniques can be a possible alternative to analyze the local coating defects and evaluate the corrosion mitigation. The analysis of active coating defects has the great advantage of giving local information, regarding the evolution of the corrosion processes (progress and mitigation) on active defects of the coating. Scanning vibrating electrode technique (SVET) and scanning the ion-selective electrode technique is used in the work of Montemor [129] to investigate current density maps in order to quantify the overall electrochemical activity and the total anodic and cathodic current densities. SVET mapping has been also employed to evaluate the effect of organic corrosion inhibitors intercalated in between the lamellae of the LDH [101]. Tedim et al. [130] investigated the electrochemical activity of MgAl-LDH in the presence and absence of vanadates by SVET and assessed also the local intensity of corrosion currents and degree of localization of the corrosion attack. The potential of SVET to assess the effectiveness of corrosion inhibitor loaded LDH has been confirmed also when co-precipitated particles are embedded in an organic coating [131].

Table 2. LDH-based systems and measured corrosion resistance properties.

LDH	Substrate	Potentiodynamic Curves			Electrochemical Impedance Spectroscopy				Ref.
		Electrolyte (NaCl)	i_{corr} sub. (A cm^{-2})	i_{corr} Film (A cm^{-2})	Electrolyte (NaCl)	Immersion Time (h)	R_{pol} (Ω cm^2)	R_{coat} (Ω cm^2)	
ZnAlNO$_3$		-	-	-	0.05	1000	10^5		[69]
ZnAlV$_2$O$_7$	2024	-	-	-			10^6	2×10^3	
MgAlNO$_3$							3.3×10^6	82	
MgAlNO$_3$							44.3×10^6	128	
MgAl-8HQ	Pure Al	3.5 wt.%	1.5×10^{-7}	1.95×10^{-8} / 1.02×10^{-9}	3.5 wt.%	336	9.3×10^7 / 3.7×10^9	9.0×10^5 / 5.2×10^7	[71]
MgAlNO$_3$	6061	-	-	-	0.05M	10	1.0×10^6	6.1×10^2	[72]
MgAl-C$_6$H$_5$COO									
AN-ZnAl									
AN-ZnAl-VO$_3$	2198	-	-	-	0.5M	-	1.0×10^7	8.6×10^2	[73]
AN-ZnAl-VO$_3$							9.7×10^6	4.9×10^3	
PEO-ZnAlVOx	2024				0.5 wt.%	72	47×10^3	47×10^3	[74]
PEO-ZnAlNO$_3$									
PEO-ZnAlVOx	2024				0.05 M	336	1.8×10^7	2.3×10^4	[75]
MgAlNO$_3$	6082	0.1 M	7.5×10^{-6}	8.3×10^{-10}	0.1 M	-		3.3×10^4	[64]
MgAlNO$_3$	6082	0.1 M	7.5×10^{-6}	1.9×10^{-11} / 6.3×10^{-10}	0.1 M	1	4.2×10^9	2.3×10^8	[76]
MgAlNO$_3$									
CaAlNO$_3$	6082	0.1	7.5×10^{-6}	7.0×10^{-10}	3.5 wt.%	-	9.9×10^4	9.9×10^4	[77]
ZnAlNO$_3$	6082	0.1	4.4×10^{-6}	1.1×10^{-7}	3.5 wt.%	1	1.2×10^5	1.2×10^5	[78]
ZnAlLa	Pure Al	3.5 wt.%		6×10^{-8}					
NiAlNO$_3$	6082	0.1	7.5×10^{-7}	1.410^{-9}	0.1	1	2.5×10^9	1.4×10^6	[79]
NiAlCO$_3$	Pure Al	3.5 wt.%	10^{-6}	10^{-9}	-	-	8.2×10^4	8.2×10^4	[80]
MgAl-oleate							6.8×10^6	8.2×10^4	
MgAl Laurate	Pure Al	-	-	-	3.5 wt.%	168	7.0×10^{11}	9.1×10^5	[82]
MgAl stearate							6.0×10^{10}	1.1×10^6	
MgAl-SA	5005	3.5 wt.%	1.3×10^{-5}	2.0×10^{-8}	-	-	1.9×10^{10}	1.9×10^{10}	[70]
ZnAlNO$_3$	6N01	3.5 wt.%	4.7×10^{-6}	5.3×10^{-5} / 4.3×10^{-8}	3.5 wt.%	168	2.3×10^2	2.4×10^{10}	[85]
ZnAl/RGO							7.4×10^3	2.3×10^2	
ZnAlNO$_3$							2.9×10^4	9.9×10^2	
ZnAlMO	2024	-	-	-	3.5 wt.%	48	9.9×10^2	9.9×10^2	[86]
ZnAlMO/GN							3.9×10^5	2.4×10^3	
LiAlNO$_3$			0.32×10^{-6}	0.19×10^{-6}			3.5×10^5	2.4×10^3	
LiNO$_3$/Vanillin	A6N01	3.5 wt.%	0.32×10^{-6}	0.03×10^{-6}	3.5 wt.%	120	3.5×10^7	3.8×10^9	[92]
MgAl-FAS-13	6061	3.5 wt.%	1.5×10^{-4}	7.9×10^{-6}	3.5 wt.%	408	3.7×10^3		[100]
MgAl-PVA	5054	-	-	-	3.5 wt.%	480	3.3×10^4	7.4×10^4	[107]
ZnAlV$_2$O$_7$	2024	-	-	-	0.5 M	1		1.0×10^4	[132]

8HQ: 8-hydroxyquinolate; C$_6$H$_5$COO: benzoate; AN: anodized; PEO: plasma electrolytic oxidation; VOx: Vanadium oxide; SA: stearic acid; RGO: Reduced graphene oxide; GN: graphene.

Table 3. LDH particles dispersed in organic/polymeric matrix, and corresponding measured corrosion resistance properties.

LDH	Substrate	Potentiodynamic Curves			Electrochemical Impedance Spectroscopy				Ref.
		Electrolyte (NaCl)	i_{corr} sub. (A cm^{-2})	i_{corr} Film (A cm^{-2})	Electrolyte (NaCl)	Immersion Time (h)	R_{pol} (Ω cm^2)	R_{coat} (Ω cm^2)	
ZnAl-V/PVA	2024	-	-	-	0.5 M	200	-	1×10^7	[50]
ZnAl-V/epoxy	2024	0.124 M	1×10^{-6}	2×10^{-8}	-	-	-	-	[51]
ZnAl/3-ABSA				1.8×10^{-7}			-	780	
ZnAl/3,4-HHBA	2024	0.5 M	-	6.4×10^{-7}			-	290	[57]
LDH/4-ABSA				4.4×10^{-7}	0.005 M	1400	-	910	
ZnAl-EDTA			-	2.9×10^{-7}			-	8×10^5	
ZnAl-CO$_3$			-	3.8×10^{-7}			-	2×10^4	
ZnAl-CrO$_4$	2024	0.5 M	-	0.69×10^{-7}	0.5 M	1608	-	4×10^5	[58]
ZnAl-Cl			-	2.4×10^{-7}			-	2×10^3	
ZnAl-Ce/sol gel	2024	-	-	-	0.05	336	-	334.9	[59]
MgAl-sol-gel	2024	-	-	-	0.1 M	210	-	300	[87]
ZnAl E3/E1	2024		4.4×10^{-5}	1.4×10^{-6}	3.5 wt.%	120	-	4.1×10^3	
ZnAl-sol-gel	-		7.6×10^{-7}	7.6×10^{-7}	-	-	-	7.6×10^3	
ZnAl-sol-gel	-	3.5 wt.%	1.8×10^{-7}	1.8×10^{-7}	-	-	-	1.6×10^4	[91]
ZnAl-sol-gel	-		2.6×10^{-7}	2.6×10^{-7}	-	-	-	4.6×10^3	

ABSA: Acetamidobenzenesulfonyl azide; HHBA: dihydroxybenzoic acid; V: Decavandate; PVA: polyvinyl alcohol; EDTA: Ethylenediaminetetraacetic acid.

4. Conclusions and Outlook

This work summarizes the significant approaches and synthetic conditions used to develop the LDHs on aluminum substrates to develop a smart coating system to protect the metallic surface from corrosion. In recent years, a lot of contributions have been made to develop compact LDH-based systems and have proven an efficient approach to protect Al alloys. It is common to synthesize LDH functional materials on aluminum surfaces to improve their corrosion resistance properties as well as obtain other multi-functional responses. The hybrid inorganic-organic coating systems, utilization, and investigation of the number of corrosion inhibitors/pigments have created a new generation of multifunctional responsive coatings, yet the size and geometry of the defects healed in accordance with the self-healing characteristics of LDHs, the controlled release of inhibitors in different reactive situations, the response of LDH on the occurrence of multiple damaging, pitting corrosion healing, and facile synthesis of defects free, low time-consuming LDH preparation are still open questions with limited solutions.

Conflicts of Interest: The authors declare no conflict of interest.

References

1. Davis, J.R. (Ed.) *Corrosion of Aluminum and Aluminum Alloys*; ASM International: Geauga, OH, USA, 1999.
2. Xhanari, K.; Finšgar, M. Organic corrosion inhibitors for aluminum and its alloys in chloride and alkaline solutions: A review. *Arab. J. Chem.* **2016**, *12*, 4646–4663. [CrossRef]
3. Liang, W.J.; Rometsch, P.A.; Cao, L.F.; Birbilis, N. General aspects related to the corrosion of 6xxx series aluminium alloys: Exploring the influence of Mg/Si ratio and Cu. *Corros. Sci.* **2013**, *76*, 119–128. [CrossRef]
4. Larsen, M.H.; Walmsley, J.C.; Lunder, O.; Mathiesen, R.H.; Nisancioglu, K. Intergranular corrosion of copper-containing AA6xxx AlMgSi aluminum alloys. *J. Electrochem. Soc.* **2008**, *155*, 550–556. [CrossRef]
5. Ye, H. An Overview of the Development of Al-Si-Alloy Based Material for Engine Applications. *J. Mater. Eng. Perform.* **2003**, *12*, 288–297. [CrossRef]
6. Chen, C.L.; West, G.; Thomson, R.C. Characterisation of intermetallic phases in multicomponent Al-Si casting alloys for engineering applications. *Mat. Sci. Forum* **2006**, *521*, 359–364. [CrossRef]
7. Donatus, U.; Thompson, G.E.; Omotoyinbo, J.A.; Alaneme, K.K.; Aribo, S.; Agbabiaka, O.G. Corrosion pathways in aluminium alloys. *Trans. Nonferrous Met. Soc. China* **2017**, *27*, 55–62. [CrossRef]
8. Tupaj, M.; Orłowicz, A.W.; Mróz, M.; Trytek, A.; Markowska, O. The Effect of Cooling Rate on Properties of Intermetallic Phase in a Complex Al-Si Alloy. *Arch. Foundry Eng.* **2016**, *16*, 125–128. [CrossRef]
9. Yasakau, K.A.; Zheludkevich, M.L.; Lamaka, S.V.; Ferreira, M.G.S. Role of intermetallic phases in localized corrosion of AA5083. *Electrochim. Acta* **2007**, *52*, 7651–7659. [CrossRef]
10. Linder, J. The influence of surrounding environment on the fatigue properties for a high pressure die cast AlSi9Cu3 alloy. *Fatigue Fract. Eng. Mater. Struct.* **2007**, *30*, 759–765. [CrossRef]
11. Ferreira, M.G.S.; Zheludkevich, M.L.; Tedim, J.; Yasakau, K.A. *Self-Healing Nanocoatings for Corrosion Control*; Woodhead Publishing Limited: Sawston, UK, 2012.
12. Makhlouf, A.S.H. *Current and Advanced Coating Technologies for Industrial Applications*; Woodhead Publishing Limited: Sawston, UK, 2011.
13. Arenas, M.A.; Conde, A.; de Damborenea, J.J. Effect of acid traces on hydrothermal sealing of anodising layers on 2024 aluminium alloy. *Electrochim. Acta* **2010**, *55*, 8704–8708. [CrossRef]
14. Venugopal, A.; Panda, R.; Manwatkar, S.; Sreekumar, K.; Krishna, L.R.; Sundararajan, G. Effect of micro arc oxidation treatment on localized corrosion behaviour of AA7075 aluminum alloy in 3.5 NaCl solution. *Trans. Nonferrous Met. Soc. China* **2012**, *22*, 700–710. [CrossRef]

15. Dalmoro, V.; Santos, J.H.Z.D.; Armelin, E.; Alemán, C.; Azambuja, D.S. A synergistic combination of tetraethylorthosilicate and multiphosphonic acid offers excellent corrosion protection to AA1100 aluminum alloy. *Appl. Surf. Sci.* **2013**, *273*, 758–768. [CrossRef]

16. Voevodin, N.N.; Kurdziel, J.W.; Mantz, R. Corrosion protection for aerospace aluminum alloys by Modified Self-assembled NAnophase Particle (MSNAP) sol-gel. *Surf. Coat. Technol.* **2006**, *201*, 1080–1084. [CrossRef]

17. Johansen, H.D.; Brett, C.M.A.; Motheo, A.J. Corrosion protection of aluminium alloy by cerium conversion and conducting polymer duplex coatings. *Corros. Sci.* **2012**, *63*, 342–350. [CrossRef]

18. Shi, H.; Han, E.H.; Liu, F.; Kallip, S. Protection of 2024-T3 aluminium alloy by corrosion resistant phytic acid conversion coating. *Appl. Surf. Sci.* **2013**, *280*, 325–331. [CrossRef]

19. Schäfer, H.; Stock, H.R. Improving the corrosion protection of aluminium alloys using reactive magnetron sputtering. *Corros. Sci.* **2005**, *47*, 953–964. [CrossRef]

20. Diesselberg, M.; Stock, H.R.; Mayr, P. Corrosion protection of magnetron sputtered TiN coatings deposited on high strength aluminium alloys. *Surf. Coat. Technol.* **2004**, *178*, 399–403. [CrossRef]

21. Lutz, A.; van den Berg, O.; van Damme, J.; Verheyen, K.; Bauters, E.; de Graeve, I.; Prez, F.E.D.; Terryn, H. A shape-recovery polymer coating for the corrosion protection of metallic surfaces. *ACS Appl. Mater. Interfaces* **2015**, *7*, 175–183. [CrossRef]

22. Williams, G.R.; O'Hare, D. Towards understanding, control and application of layered double hydroxide chemistry. *J. Mater. Chem.* **2006**, *16*, 3065–3074. [CrossRef]

23. Qu, J.E.; Chen, G.; Wang, H.R.; Nie, D.J. Effect of water content on corrosion inhibition behavior of self-assembled TDPA on aluminum alloy surface. *Trans. Nonferrous Met. Soc. China* **2013**, *23*, 3137–3144. [CrossRef]

24. Zuo, K.; Wang, X.; Liu, W.; Zhao, Y. Preparation and characterization of Ce-silane-ZrO2 composite coatings on 1060 aluminum. *Trans. Nonferrous Met. Soc. China* **2014**, *24*, 1474–1480. [CrossRef]

25. Newman, S.P.; Jones, W. Synthesis, characterization and applications of layered double hydroxides containing organic guests. *New J. Chem.* **1998**, *22*, 105–115. [CrossRef]

26. Oh, J.M.; Biswick, T.T.; Choy, J.H. Layered nanomaterials for green materials. *J. Mater. Chem.* **2009**, *19*, 2553–2563. [CrossRef]

27. Evans, D.G.; Slade, R.C.T. Structural aspects of layered double hydroxides. *Struct. Bond.* **2005**, *119*, 1–87.

28. Yu, J.; Liu, J.; Clearfield, A.; Sims, J.E.; Speiegle, M.T.; Suib, S.L.; Sun, L. Synthesis of layered double hydroxide single-layer nanosheets in formamide. *Inorg. Chem.* **2016**, *55*, 12036–12041. [CrossRef] [PubMed]

29. Liu, Z.L.; Tian, D.Y.; Li, S.P.; Li, X.D.; Lu, T.H. MTX/LDHs hybrids synthesized from reverse microemulsions: Particle control and bioassay study. *Int. J. Pharm.* **2014**, *473*, 414–425. [CrossRef]

30. Chitrakar, R.; Makita, Y.; Sonoda, A.; Hirotsu, T. Synthesis of a novel layered double hydroxides [MgAl$_4$(OH)$_{12}$](Cl)$_2$·2.4H$_2$O and its anion-exchange properties. *J. Hazard. Mater.* **2011**, *185*, 1435–1439. [CrossRef]

31. Cai, X.; Shen, X.; Ma, L.; Ji, Z.; Xu, C.; Yuan, A. Solvothermal synthesis of NiCo-layered double hydroxide nanosheets decorated on RGO sheets for high performance supercapacitor. *Chem. Eng. J.* **2015**, *268*, 251–259. [CrossRef]

32. Iqbal, M.A.; Asghar, H.; Iqbal, M.A.; Fedel, M. Sorption of As(V) from aqueous solution using in situ growth MgAl–NO3 layered double hydroxide thin film developed on AA6082. *SN Appl. Sci.* **2019**, *1*, 1–9. [CrossRef]

33. Laipan, M.; Fu, H.; Zhu, R.; Sun, L.; Steel, R.M.; Ye, S.; Zhu, J.; He, H. Calcined Mg/Al-LDH for acidic wastewater treatment: Simultaneous neutralization and contaminant removal. *Appl. Clay Sci.* **2018**, *153*, 46–53. [CrossRef]

34. Laipan, M.; Fu, H.; Zhu, R.; Sun, L.; Zhu, J.; He, H. Converting Spent Cu/Fe Layered Double Hydroxide into Cr(VI) Reductant and Porous Carbon Material. *Sci. Rep.* **2017**, *7*, 1–11. [CrossRef]

35. Xu, Y.; Huang, W.; Chen, X.; Ge, F.; Zhu, R.; Sun, L. Self-assembled ZnAl-LDH/PMo12 nano-hybrids as effective catalysts on the degradation of methyl orange under room temperature and ambient pressure. *Appl. Catal. A* **2018**, *550*, 206–213. [CrossRef]

36. Yang, J.H.; Han, Y.S.; Park, M.; Park, T.; Hwang, S.J.; Choy, J.H. New inorganic-based drug delivery system of indole-3-acetic acid-layered metal hydroxide nanohybrids with controlled release rate. *Chem. Mater.* **2007**, *19*, 2679–2685. [CrossRef]

37. Guo, X.; Zhang, F.; Peng, Q.; Xu, S.; Lei, X.; Evans, D.G.; Duan, X. Layered double hydroxide/eggshell membrane: An inorganic biocomposite membrane as an efficient adsorbent for Cr(VI) removal. *Chem. Eng. J.* **2011**, *166*, 81–87. [CrossRef]

38. Guo, L.; Wu, W.; Zhou, Y.; Zhang, F.; Zeng, R.; Zeng, J. Layered double hydroxide coatings on magnesium alloys: A review. *J. Mater. Sci. Technol.* **2018**, *34*, 1455–1466. [CrossRef]

39. Okamoto, K.; Iyi, N.; Sasaki, T. Factors affecting the crystal size of the MgAl-LDH (layered double hydroxide) prepared by using ammonia-releasing reagents. *Appl. Clay Sci.* **2007**, *37*, 23–31. [CrossRef]

40. Iqbal, M.; Fedel, M. Effect of Synthesis Conditions on the Controlled Growth of MgAl–LDH Corrosion Resistance Film: Structure and Corrosion Resistance Properties. *Coatings* **2019**, *9*, 30. [CrossRef]

41. Bukhtiyarova, M.V. A review on effect of synthesis conditions on the formation of layered double hydroxides. *J. Solid State Chem.* **2019**, *269*, 494–506. [CrossRef]

42. Miyata, S. Anion-exchange properties of hydrotalcite-like compounds. *Clay Clay Miner.* **1983**, *31*, 305–311. [CrossRef]

43. Bravo-Suárez, J.J.; Páez-Mozo, E.A.; Oyama, S.T. Review of the synthesis of layered double hydroxides: A thermodynamic approach. *Quim. Nova* **2004**, *27*, 601–604. [CrossRef]

44. Yan, K.; Wu, G.; Jin, W. Recent Advances in the Synthesis of Layered, Double-Hydroxide-Based Materials and Their Applications in Hydrogen and Oxygen Evolution. *Energy Technol.* **2016**, *4*, 354–368. [CrossRef]

45. Chubar, N.; Gilmour, R.; Gerda, V.; Mičušík, M.; Omastova, M.; Heister, K.; Man, P.; Fraissard, J.; Zaitsev, V. Layered double hydroxides as the next generation inorganic anion exchangers: Synthetic methods versus applicability. *Adv. Colloid Interface Sci.* **2017**, *245*, 62–80. [CrossRef] [PubMed]

46. Wang, Q.; Ohare, D. Recent advances in the synthesis and application of layered double hydroxide (LDH) nanosheets. *Chem. Rev.* **2012**, *112*, 4124–4155. [CrossRef] [PubMed]

47. Nalawade, P.; Aware, B.; Kadam, V.J.; Hirlekar, R.S. Layered double hydroxides: A review. *J. Sci. Ind. Res.* **2009**, *68*, 267–272.

48. Theiss, F.L.; Ayoko, G.A.; Frost, R.L. Synthesis of layered double hydroxides containing Mg^{2+}, Zn^{2+}, Ca^{2+} and Al^{3+} layer cations by co-precipitation methods—A review. *Appl. Surf. Sci.* **2016**, *383*, 200–213. [CrossRef]

49. Salak, A.N.; Tedim, J.; Kuznetsova, A.I.; Ribeiro, J.L.; Vieira, L.G.; Zheludkevich, M.L.; Ferreira, M.G. Comparative X-ray diffraction and infrared spectroscopy study of Zn-Al layered double hydroxides: Vanadate vs nitrate. *Chem. Phys.* **2012**, *397*, 102–108. [CrossRef]

50. Buchheit, R.G.; Guan, H.; Mahajanam, S.; Wong, F. Active corrosion protection and corrosion sensing in chromate-free organic coatings. *Prog. Org. Coat.* **2003**, *4*, 174–182. [CrossRef]

51. Mahajanam, S.P.V.; Buchheit, R.G. Characterization of inhibitor release from Zn-Al-[V10 O28]6- hydrotalcite pigments and corrosion protection from hydrotalcite-pigmented epoxy coatings. *Corrosion* **2008**, *64*, 230–240. [CrossRef]

52. Williams, G.; McMurray, H.N. Anion-exchange inhibition of filiform corrosion on organic coated AA2024-T3 aluminum alloy by hydrotalcite-like pigments. *Electrochem. Solid-State Lett.* **2003**, *6*, 9–11. [CrossRef]

53. Williams, G.; McMurray, H.N. Inhibition of filiform corrosion on polymer coated AA2024-T3 by hydrotalcite-like pigments incorporating organic anions. *Electrochem. Solid-State Lett.* **2004**, *7*, 13–15. [CrossRef]

54. Michailidou, E.; McMurray, H.N.; Williams, G. Inhibition of filiform corrosion on organic-coated magnesium-containing galvanized steel by smart-release ion exchange pigments. *ECS Trans.* **2017**, *80*, 585–591. [CrossRef]

55. Poznyak, S.K.; Tedim, J.; Rodrigues, L.M.; Salak, A.N.; Zheludkevich, M.L.; Dick, L.F.; Ferreira, M.G. Novel inorganic host layered double hydroxides intercalated with guest organic inhibitors for anticorrosion applications. *ACS Appl. Mater. Interfaces* **2009**, *1*, 2353–2362. [CrossRef]

56. Zheludkevich, M.L.; Poznyak, S.K.; Rodrigues, L.M.; Raps, D.; Hack, T.; Dick, L.F.; Nunes, T.; Ferreira, M.G.S. Active protection coatings with layered double hydroxide nanocontainers of corrosion inhibitor. *Corros. Sci.* **2010**, *52*, 602–611. [CrossRef]

57. Stimpfling, T.; Leroux, F.; Hintze-Bruening, H. Organo-modified layered double hydroxide in coating formulation to protect AA2024 from corrosion. *Colloids Surf., A* **2014**, *458*, 147–154. [CrossRef]

58. Stimpfling, T.; Leroux, F.; Hintze-Bruening, H. Unraveling EDTA corrosion inhibition when interleaved into Layered Double Hydroxide epoxy filler system coated onto aluminum AA 2024. *Appl. Clay Sci.* **2013**, *84*, 32–41. [CrossRef]

59. Liu, J.; Zhang, Y.; Yu, M.; Li, S.; Xue, B.; Yin, X. Influence of embedded ZnAlCe-NO^{3-} layered double hydroxides on the anticorrosion properties of sol-gel coatings for aluminum alloy. *Prog. Org. Coat.* **2015**, *81*, 93–100. [CrossRef]

60. Galvão, T.L.; Neves, C.S.; Caetano, A.P.; Maia, F.; Mata, D.; Malheiro, E.; Ferreira, M.J.; Bastos, A.C.; Salak, A.N.; Gomes, J.R.; et al. Control of crystallite and particle size in the synthesis of layered double hydroxides: Macromolecular insights and a complementary modeling tool. *J. Colloid Interf. Sci.* **2016**, *468*, 86–94. [CrossRef]

61. Buchheit, R.G., Jr.; Stoner, G.E. Method for increasing the corrosion resistance of aluminum and aluminum alloys. US Patent number RE35576, 29 July 1997.

62. Zhang, Y.; Li, Y.; Ren, Y.; Wang, H.; Chen, F. Double-doped LDH films on aluminum alloys for active protection. *Mater. Lett.* **2017**, *192*, 33–35. [CrossRef]

63. Zhou, B.; Wei, X.; Wang, Y.; Huang, Q.; Hong, B.; Wei, Y. Effect of lanthanum addition on microstructures and corrosion behavior of ZnAl-LDHs film of 6061 aluminum alloys. *Surf. Coat. Technol.* **2019**, *379*, 125056. [CrossRef]

64. Iqbal, M.A.; Fedel, M. The effect of the surface morphologies on the corrosion resistance of in situ growth MgAl-LDH based conversion film on AA6082. *Surf. Coat. Technol.* **2018**, *352*, 166–174. [CrossRef]

65. Iqbal, M.A.; Sun, L.; Fedel, M. Synthesis of novel cone—shaped CaAl - LDH directly on aluminum alloy by a facile urea hydrolysis method. *SN Appl. Sci.* **2019**, *1*, 1415. [CrossRef]

66. Serdechnova, M.; Mohedano, M.; Bouali, A.C.; Höche, D.; Kuznetsov, B.; Karpushenkov, S.; Blawert, C.; Zheludkevich, M.L. Role of Phase Composition of PEO Coatings on AA2024 for In-Situ LDH Growth. *Coatings* **2017**, *7*, 190. [CrossRef]

67. Bouali, A.C.; Straumal, E.A.; Serdechnova, M.; Wieland, D.C.; Starykevich, M.; Blawert, C.; Hammel, J.U.; Lermontov, S.A.; Ferreira, M.G.; Zheludkevich, M.L. Applied Surface Science Layered double hydroxide based active corrosion protective sealing of plasma electrolytic oxidation/sol-gel composite coating on AA2024. *Appl. Surf. Sci.* **2019**, *494*, 829–840. [CrossRef]

68. Mikhailau, A.; Maltanava, H.; Poznyak, S.K.; Salak, A.N.; Zheludkevich, M.L.; Yasakau, K.A.; Ferreira, M.G.S. One-step synthesis and growth mechanism of nitrate intercalated ZnAl LDH conversion coatings on zinc. *Chem. Commun.* **2019**, *55*, 6878–6881. [CrossRef] [PubMed]

69. Tedim, J.; Zheludkevich, M.L.; Salak, A.N.; Lisenkov, A.; Ferreira, M.G.S. Nanostructured LDH-container layer with active protection functionality. *J. Mater. Chem.* **2011**, *21*, 15464–15470. [CrossRef]

70. Zhang, F.; Zhao, L.; Chen, H.; Xu, S.; Evans, D.G.; Duan, X. Corrosion resistance of superhydrophobic layered double hydroxide films on aluminum. *Angew. Chemie Int. Ed.* **2008**, *47*, 2466–2469. [CrossRef]

71. Wang, L.; Zhang, K.; He, H.; Sun, W.; Zong, Q.; Liu, G. Enhanced corrosion resistance of MgAl hydrotalcite conversion coating on aluminum by chemical conversion treatment. *Surf. Coat. Technol.* **2013**, *235*, 484–488. [CrossRef]

72. Kaseem, M.; Ko, Y.G. Benzoate intercalated Mg-Al-layered double hydroxides (LDHs) as efficient chloride traps for plasma electrolysis coatings. *J. Alloys Compd.* **2019**, *787*, 772–778. [CrossRef]

73. Li, Y.; Li, S.; Zhang, Y.; Yu, M.; Liu, J. Enhanced protective Zn-Al layered double hydroxide film fabricated on anodized 2198 aluminum alloy. *J. Alloys Compd.* **2015**, *630*, 29–36. [CrossRef]

74. Serdechnova, M.; Mohedano, M.; Kuznetsov, B.; Mendis, C.L.; Starykevich, M.; Karpushenkov, S.; Tedim, J.; Ferreira, M.G.; Blawert, C.; Zheludkevich, M.L. PEO coatings with active protection based on in-situ formed LDH-nanocontainers. *J. Electrochem. Soc.* **2017**, *164*, C36–C45. [CrossRef]

75. Kuznetsov, B.; Serdechnova, M.; Tedim, J.; Starykevich, M.; Kallip, S.; Oliveira, M.P.; Hack, T.; Nixon, S.; Ferreira, M.G.; Zheludkevich, M.L. Sealing of tartaric sulfuric (TSA) anodized AA2024 with nanostructured LDH layers. *RSC Adv.* **2016**, *6*, 13942–13952. [CrossRef]

76. Iqbal, M.A.; Fedel, M. Effect of operating parameters on the structural growth of ZnAl layered double hydroxide on AA6082 and corresponding corrosion resistance properties. *J. Coat. Technol. Res.* **2019**, *16*, 1423–1433. [CrossRef]

77. Iqbal, M.A.; Sun, L.; LaChance, A.M.; Ding, H.; Fedel, M. In situ growth of a CaAl-NO 3—layered double hydroxide film directly on an aluminum alloy for corrosion resistance. *Dalton Trans.* **2020**, *49*, 3956–3964. [CrossRef] [PubMed]

78. Cao, Y.; Zheng, D.; Li, X.; Lin, J.; Wang, C.; Dong, S.; Lin, C. Enhanced Corrosion Resistance of Superhydrophobic Layered Double Hydroxide Films with Long-Term Stability on Al Substrate. *ACS Appl. Mater. Interfaces* **2018**, *10*, 15150–15162. [CrossRef] [PubMed]

79. Iqbal, M.A.; Sun, M.A.L.; Asghar, H.; Fedel, M. Chlorides Entrapment Capability of Various In-Situ Grown NiAl-LDHs: Structural and Corrosion Resistance Properties. *Coatings* **2020**, *10*, 384. [CrossRef]

80. Liu, Y.; Yu, T.; Cai, R.; Li, Y.; Yang, W.; Caro, J. One-pot synthesis of NiAl-CO$_3$ LDH anti-corrosion coatings from CO$_2$-saturated precursors. *RSC Adv.* **2015**, *5*, 29552–29557. [CrossRef]

81. Zhang, F.; Zhang, C.L.; Song, L.; Zeng, R.C.; Liu, Z.G.; Cui, H.Z. Corrosion of in-situ grown MgAl-LDH coating on aluminum alloy. *Trans. Nonferrous Met. Soc. China* **2015**, *25*, 3498–3504. [CrossRef]

82. Wang, Y.; Zhang, D.; Lu, Z. Hydrophobic Mg-Al layered double hydroxide film on aluminum: Fabrication and microbiologically influenced corrosion resistance properties. *Colloids Surf. A* **2015**, *474*, 44–51. [CrossRef]

83. Guo, X.; Xu, S.; Zhao, L.; Lu, W.; Zhang, F.; Evans, D.G.; Duan, X. One-step hydrothermal crystallization of a layered double hydroxide/alumina bilayer film on aluminum and its corrosion resistance properties. *Langmuir* **2009**, *25*, 9894–9897. [CrossRef]

84. Zhang, F.; Zhang, C.L.; Song, L.; Zeng, R.C.; Cui, L.Y.; Cui, H.Z. Corrosion resistance of superhydrophobic mg-al layered double hydroxide coatings on aluminum alloys. *Acta Metall. Sin. English Lett.* **2015**, *28*, 1373–1381. [CrossRef]

85. Luo, X.; Yuan, S.; Pan, X.; Zhang, C.; Du, S.; Liu, Y. Synthesis and Enhanced Corrosion Protection Performance of Reduced Graphene Oxide Nanosheet/ZnAl Layered Double Hydroxide Composite Films by Hydrothermal Continuous Flow Method. *ACS Appl. Mater. Interfaces* **2017**, *9*, 18263–18275. [CrossRef] [PubMed]

86. Zhang, Y.; Yu, P.; Wang, J.; Li, Y.; Chen, F.; Wei, K.; Zuo, Y. LDHs/graphene film on aluminum alloys for active protection. *Appl. Surf. Sci.* **2018**, *433*, 927–933. [CrossRef]

87. Álvarez, D.; Collazo, A.; Hernández, M.; Nóvoa, X.R.; Pérez, C. Characterization of hybrid sol-gel coatings doped with hydrotalcite-like compounds to improve corrosion resistance of AA2024-T3 alloys. *Prog. Org. Coat.* **2010**, *68*, 91–99. [CrossRef]

88. Li, W.; Zhang, X.; Yang, J.; Miao, F. In situ growth of superhydrophobic and icephobic films with micro/nanoscale hierarchical structures on the aluminum substrate. *J. Colloid Interface Sci.* **2013**, *410*, 165–171. [CrossRef]

89. Mohedano, M.; Serdechnova, M.; Starykevich, M.; Karpushenkov, S.; Bouali, A.C. Active protective PEO coatings on AA2024: Role of voltage on in-situ LDH growth. *Mater. Des.* **2017**, *120*, 36–46. [CrossRef]

90. Li, Y.; Li, S.; Zhang, Y.; Yu, M.; Liu, J. Fabrication of superhydrophobic layered double hydroxides films with different metal cations on anodized aluminum 2198 alloy. *Mater. Lett.* **2015**, *142*, 137–140. [CrossRef]

91. Subasri, R.; Raju, K.S.; Reddy, D.S.; Jyothirmayi, A.; Ijeri, V.S.; Prakash, O.; Gaydos, S.P. Environmentally friendly Zn–Al layered double hydroxide (LDH)-based sol–gel corrosion protection coatings on AA 2024-T3. *J. Coat. Technol. Res.* **2019**, *16*, 1447–1463. [CrossRef]

92. Lin, K.; Luo, X.; Pan, X.; Zhang, C.; Liu, Y. Enhanced corrosion resistance of LiAl-layered double hydroxide (LDH) coating modified with a Schiff base salt on aluminum alloy by one step in-situ synthesis at low temperature. *Appl. Surf. Sci.* **2019**, *463*, 1085–1096. [CrossRef]

93. Liang, Z.; Ma, Y.; Li, K.; Liao, Y.; Yang, B.; Liu, L.; Zhu, P. Formation of layered double hydroxides fi lm on AA2099-T83 Al-Cu-Li alloy and its e ff ect on corrosion resistance. *Surf. Coat. Technol.* **2019**, *378*, 124967. [CrossRef]

94. Radha, A.V.; Kamath, P.V.; Shivakumara, C. Mechanism of the anion exchange reactions of the layered double hydroxides (LDHs) of Ca and Mg with Al. *Solid State Sci.* **2005**, *7*, 1180–1187. [CrossRef]

95. Allada, R.; Navrotsky, A. Thermochemistry and Aqueous Solubilities of Hydrotalcite-Like Solids. *Science* **2002**, *296*, 721–723. [CrossRef] [PubMed]

96. Tedim, J.; Kuznetsova, A.; Salak, A.N.; Montemor, F.; Snihirova, D.; Pilz, M.; Zheludkevich, M.L.; Ferreira, M.G. Zn-Al layered double hydroxides as chloride nanotraps in active protective coatings. *Corros. Sci.* **2012**, *55*, 1–4. [CrossRef]

97. Tedim, J.; Zheludkevich, M.L.; Bastos, A.C.; Salak, A.N.; Lisenkov, A.D.; Ferreira, M.G.S. Influence of preparation conditions of Layered Double Hydroxide conversion films on corrosion protection. *Electrochim. Acta* **2014**, *117*, 164–171. [CrossRef]

98. Neves, C.S.; Bastos, A.C.; Salak, A.N.; Starykevich, M.; Rocha, D.; Zheludkevich, M.L.; Cunha, A.; Almeida, A.; Tedim, J.; Ferreira, M.G. Layered Double Hydroxide Clusters as Precursors of Novel Multifunctional Layers: A Bottom-Up Approach. *Coatings* **2019**, *9*, 328. [CrossRef]

99. Chen, H.; Zhang, F.; Fu, S.; Duan, X. In situ microstructure control of oriented layered double hydroxide monolayer films with curved hexagonal crystals as superhydrophobic materials. *Adv. Mater.* **2006**, *18*, 3089–3093. [CrossRef]

100. Wang, F.; Guo, Z. Insitu growth of durable superhydrophobic Mg e Al layered double hydroxides nanoplatelets on aluminum alloys for corrosion resistance. *J. Alloys Compd.* **2018**, *767*, 382–391. [CrossRef]

101. Iqbal, M.A.; Fedel, M. Ordering and disordering of in situ grown MgAl-layered double hydroxide and its effect on the structural and corrosion resistance properties. *Int. J. Miner. Metall. Mater.* **2019**, *26*, 1570–1577. [CrossRef]

102. Kovanda, F.; Masatova, P.; Novotna, P.; Jratova, K. The formation of layered double hydroxides on alumina surface. *Clays Clay Miner.* **2009**, *57*, 425–432. [CrossRef]

103. Chen, F.; Yu, P.; Zhang, Y. Healing effects of LDHs nanoplatelets on MAO ceramic layer of aluminum alloy. *J. Alloys Compd.* **2017**, *711*, 342–348. [CrossRef]

104. Wang, L.; Li, B.; Zhao, X.; Chen, C.; Cao, J. Effect of Rare Earth Ions on the Properties of Composites Composed of Ethylene Vinyl Acetate Copolymer and Layered Double Hydroxides. *PLoS ONE* **2012**, *7*, e37781. [CrossRef]

105. Van de Sanden, M.C.; Severens, R.J.; Bastiaanssen, J.; Schram, D.C. High-quality a-Si:H growth at high rate using an expanding thermal plasma. *Surf. Coat. Technol.* **1997**, *97*, 719–722. [CrossRef]

106. Lyon, S.B.; Bingham, R.; Mills, D.J. Progress in Organic Coatings Advances in corrosion protection by organic coatings: What we know and what we would like to know. *Prog. Org. Coat.* **2017**, *102*, 2–7. [CrossRef]

107. Imanieh, I.; Afshar, A. Corrosion protection of aluminum by smart coatings containing layered double hydroxide (LDH) nanocontainers. *J. Mater. Res. Technol.* **2019**, *8*, 3004–3023. [CrossRef]

108. Zhang, Y.; Liu, J.; Li, Y.; Yu, M.; Yin, X.; Li, S. Enhancement of active anticorrosion via Ce-doped Zn-Al layered double hydroxides embedded in sol-gel coatings on aluminum alloy. *J. Wuhan Univ. Technol. Mater. Sci. Ed.* **2017**, *32*, 1199–1204. [CrossRef]

109. ISO. *ISO. 8407: 2009 (E). Corrosion of Metals and Alloys—Removal of Corrosion Products from Corrosion Test Specimens*; International Standards Organization: Geneva, Switzerland, 2009.

110. Bendinelli, E.V.; Aoki, I.V.; Barcia, O.; Margarit-mattos, I.C.P. Kinetic aspects of Mg-Al layered double hydroxides influencing smart corrosion protective behavior. *Mater. Chem. Phys.* **2019**, *238*, 121883. [CrossRef]

111. Rojas, R.; Jimenez-kairuz, A.F.; Manzo, R.H.; Giacomelli, C.E. Colloids and Surfaces A: Physicochemical and Engineering Aspects Release kinetics from LDH-drug hybrids: Effect of layers stacking and drug solubility and polarity. *Colloids Surf. A* **2014**, *463*, 37–43. [CrossRef]

112. Gao, X.; Lei, L.; Hare, D.O.; Xie, J.; Gao, P.; Chang, T. Journal of Solid State Chemistry Intercalation and controlled release properties of vitamin C intercalated layered double hydroxide. *J. Solid State Chem.* **2013**, *203*, 174–180. [CrossRef]

113. Khodam, F.; Rezvani, Z.; Amani-ghadim, A.R. Journal of Industrial and Engineering Chemistry Enhanced adsorption of Acid Red 14 by co-assembled LDH/MWCNTs nanohybrid: Optimization, kinetic and isotherm. *J. Ind. Eng. Chem.* **2014**, *21*, 1286–1294. [CrossRef]

114. Szauer, T. Impedance measurements for the evaluation of protective nonmetallic coatings. *Prog. Org. Coat.* **1982**, *10*, 171–183. [CrossRef]

115. Mansfeld, F.; Kendig, M.W.; Tsai, S. Evaluation of corrosion behavior of coated metals with ac impedance measurements. *Corrosion* **1982**, *38*, 478–485. [CrossRef]

116. MacDonald, D.D. Reflections on the history of electrochemical impedance spectroscopy. *Electrochim. Acta* **2006**, *51*, 1376–1388. [CrossRef]

117. Bacon, R.C.; Smith, J.J.; Rugg, F.M. Electrolytic Resistance in Evaluating Protective Merit of Coatings on Metals. *Ind. Eng. Chem.* **1948**, *40*, 161–167. [CrossRef]

118. Murray, J.N. Electrochemical test methods for evaluating organic coatings on metals: An update. Part I. Introduction and generalities regarding electrochemical testing of organic coatings. *Prog. Org. Coat.* **1997**, *30*, 225–233. [CrossRef]

119. Amirudin, A.; Thierry, D. Application of electrochemical impedance spectroscopy to study the degradation of polymer-coated metals. *Prog. Org. Coat.* **1995**, *26*, 1–28. [CrossRef]

120. Macdonald, J.R.; Hill, C.; Hooper, A. Company Analysis of hydrogen-doped lithium nitride admittance data. *Solid State Ionics* **1982**, *6*, 65–77. [CrossRef]

121. Boukamp, B.A. A non linear leasts squares fit procedure for analysis of immittance data of electrochemical systems. *Solid State Ionics* **1985**, *20*, 31–44. [CrossRef]

122. Kelly, G.J. Corrosion Engineering-Practices vs Principles. In *Engineering Conference 1984: Conference Papers*; Institution of Engineers: Brisbane, Australia, 1984; p. 376.

123. Jorcin, J.B.; Orazem, M.E.; Pébère, N.; Tribollet, B. CPE analysis by local electrochemical impedance spectroscopy. *Electrochim. Acta* **2006**, *51*, 1473–1479. [CrossRef]

124. Walter, G.W. The application of impedance spectroscopy to study the uptake of sodium chloride solution in painted metals. *Corros. Sci.* **1991**, *32*, 1041–1058. [CrossRef]

125. Fréchette, E.; Compécre, C.; Ghali, E. Evaluation of the corrosion resistance of painted steels by impedance measurements. *Corros. Sci.* **1992**, *33*, 1067–1081. [CrossRef]

126. Bierwagen, G.; Allahar, K.; Hinderliter, B.; Simões, A.M.P.; Tallman, D.; Croll, S. Ionic liquid enhanced electrochemical characterization of organic coatings. *Prog. Org. Coat.* **2008**, *63*, 250–259. [CrossRef]

127. Amand, S.; Musiani, M.; Orazem, M.E.; Pébère, N.; Tribollet, B.; Vivier, V. Electrochimica Acta Constant-phase-element behavior caused by inhomogeneous water uptake in anti-corrosion coatings. *Electrochim. Acta* **2013**, *87*, 693–700. [CrossRef]

128. Roberge, P.R. *Corrosion Engineering: Principles and Practice*; McGraw-Hill: New York, NY, USA, 2009.

129. Montemor, M.F.; Snihirova, D.V.; Taryba, M.G.; Lamaka, S.V.; Kartsonakis, I.A.; Balaskas, A.C.; Kordas, G.C.; Tedim, J.; Kuznetsova, A.; Zheludkevich, M.L. Evaluation of self-healing ability in protective coatings modified with combinations of layered double hydroxides and cerium molibdate nanocontainers filled with corrosion inhibitors. *Electrochim. Acta* **2012**, *60*, 31–40. [CrossRef]

130. Tedim, J.; Bastos, A.C.; Kallip, S.; Zheludkevich, M.L.; Ferreira, M.G.S. Corrosion protection of AA2024-T3 by LDH conversion films. Analysis of SVET results. *Electrochim. Acta* **2016**, *210*, 215–224. [CrossRef]

131. Zadeh, M.A.; Tedim, J.; Zheludkevich, M.; van der Zwaag, S.; Garcia, S.J. Synergetic active corrosion protection of AA2024-T3 by 2D- anionic and 3D- cationic nanocontainers loaded with Ce and mercaptobenzothiazole. *Corros. Sci.* **2018**, *135*, 35–45. [CrossRef]

132. Yasakau, K.A.; Kuznetsova, A.; Kallip, S.; Starykevich, M.; Tedim, J.; Ferreira, M.G.; Zheludkevich, M.L. A novel bilayer system comprising LDH conversion layer and sol-gel coating for active corrosion protection of AA2024. *Corros. Sci.* **2018**, *143*, 299–313. [CrossRef]